



Measurement of the Differential Cross Section for Isolated Prompt Photon Production in pp Collisions at 7 TeV

The CMS Collaboration*

Abstract

A measurement of the differential cross section for the inclusive production of isolated prompt photons in proton-proton collisions at a centre-of-mass energy of 7 TeV is presented. The data sample corresponds to an integrated luminosity of 36 pb^{-1} recorded by the CMS detector at the LHC. The measurement covers the pseudorapidity range $|\eta| < 2.5$ and the transverse energy range $25 < E_T < 400 \text{ GeV}$, corresponding to the kinematic region $0.007 < x_T < 0.114$. Photon candidates are identified with two complementary methods, one based on photon conversions in the silicon tracker and the other on isolated energy deposits in the electromagnetic calorimeter. The measured cross section is presented as a function of E_T in four pseudorapidity regions. The next-to-leading-order perturbative QCD calculations are consistent with the measured cross section.

Submitted to Physical Review D

*See Appendix A for the list of collaboration members

1 Introduction

The measurement of isolated prompt photon production in proton-proton collisions provides a test of perturbative quantum chromodynamics (pQCD) [1–4]. The cross section measured in pp collisions also serves as a reference for similar measurements in heavy ion collision data [5]. In addition, isolated prompt photon production represents a background to searches for new phenomena involving photons in the final state, including Higgs boson production [6]. At the Large Hadron Collider (LHC) [7], a significant increase of centre-of-mass energy with respect to previous collider experiments [8–13] allows for the exploration of new kinematic regions in the hard scattering processes in hadron-hadron collisions. In high-energy pp collisions, single prompt photons are produced directly in qg Compton scattering and $q\bar{q}$ annihilation, and in the fragmentation of partons with large transverse momentum. Photons are also produced in the decay of hadrons, mainly π^0 and η mesons, which can mimic prompt production. This background contamination can be estimated from data using photon identification characteristics, such as electromagnetic shower profile, extra energy surrounding the photon candidate (called “isolation sum” in this article), or kinematic variables of converted photons.

Both the CMS and ATLAS Collaborations have performed measurements of the differential cross section of isolated prompt photon production with data collected in 2010 [14–16]. The CMS Collaboration reported a measurement for photons with $21 < E_T < 300$ GeV and $|\eta| < 1.45$ with an integrated luminosity of 2.9 pb^{-1} and exploited the electromagnetic shower profile to estimate the background contribution [14]. Here, $E_T = E \sin \theta$ and $\eta = -\ln[\tan(\theta/2)]$, where E is the photon energy and θ is the polar angle of the photon momentum measured with respect to the counterclockwise beam direction. The measurement reported in this paper extends the previous CMS measurement to wider ranges of transverse energy ($E_T = 25\text{--}400$ GeV) and pseudorapidity ($|\eta| < 2.5$), corresponding to the kinematic region $0.007 < x_T < 0.114$, where $x_T = 2E_T/\sqrt{s}$.

The background contribution to isolated photons is estimated with two methods. The “photon conversion method” uses the variable E_T/p_T , the ratio of the transverse energy measured in the electromagnetic calorimeter to the transverse momentum measured in the tracker for converted photons. The “isolation method” uses the variable ISO, the isolation sum measured in the tracker and the electromagnetic and hadronic calorimeters. The weighted average of the differential cross sections measured with the two methods is reported as a function of E_T in four intervals of pseudorapidity: $|\eta| < 0.9$, $0.9 < |\eta| < 1.44$, $1.57 < |\eta| < 2.1$, and $2.1 < |\eta| < 2.5$. The size of the converted-photon sample is limited due to the probability for a photon to convert before reaching the CMS electromagnetic calorimeter and the relatively small conversion reconstruction efficiency. On the other hand, the signal purity obtained with the photon conversion method is very high at low photon E_T , while the isolation method is less effective at separating signal from background at low photon E_T . A combination of the cross section measurements minimises statistical and systematic uncertainties and yields better overall performance.

This paper is organised as follows. Section 2 describes the relevant CMS detector components. Sections 3, 4, and 5 list the data and simulation samples, the event selections, and the photon identification criteria that are applied in the analysis, respectively. Sections 6 and 7 detail the methods used to extract the signal photon yield and the estimation of signal efficiency. Section 8 describes the sources of systematic uncertainties on the cross section measurement and Section 9 presents the measured differential cross section. Section 10 discusses the comparison of experimental measurements with next-to-leading-order (NLO) pQCD calculations.

2 The CMS Detector

The CMS detector is a general purpose detector built to explore physics at the TeV scale and is described in detail in Ref. [17]. A brief description of the main components that are relevant to the present analysis is provided here.

The electromagnetic calorimeter (ECAL) consists of nearly 76 000 lead tungstate crystals that provide coverage in pseudorapidity $|\eta| < 1.479$ in a cylindrical barrel region and $1.479 < |\eta| < 3.0$ in two endcap regions. The crystals are $25.8 X_0$ long in the barrel and $24.7 X_0$ long in the endcaps, where X_0 denotes the radiation length. In the barrel region, the transverse distance from the interaction point to the front face of crystals, with a size of $22 \times 22 \text{ mm}^2$, is 1.29 m, corresponding to a granularity of $\Delta\eta \times \Delta\phi = 0.0174 \times 0.0174$. In the endcap region, the front face of the crystals is $28.62 \times 28.62 \text{ mm}^2$ and the distance from the interaction point to the front face is 3.15 m. Throughout this paper, ϕ is the azimuthal angle measured in radians in the plane transverse to the beam, from the direction pointing to the centre of the LHC ring toward the upward direction. A preshower detector consisting of two planes of silicon strip sensors that are interleaved with a total of $3 X_0$ of lead ($2 X_0$ in the front and $1 X_0$ after the first silicon plane) is located in front of the ECAL endcaps, covering $1.653 < |\eta| < 2.6$. Avalanche photodiodes (APDs) are used to detect the scintillation light in the barrel region, while vacuum phototriodes are used in the endcap region. The ECAL has an ultimate energy resolution better than 0.5% for unconverted photons with E_T above 100 GeV [18]. In 2010 collision data, for $E_T > 20 \text{ GeV}$, this resolution is already better than 1% in the barrel [19].

The ECAL is surrounded by a brass/scintillator sampling hadronic calorimeter (HCAL) with a coverage up to $|\eta| < 3$. The scintillation light is converted by wavelength-shifting fibres that are read out with hybrid photodiodes. The HCAL is subdivided into towers with a segmentation of $\Delta\eta \times \Delta\phi = 0.087 \times 0.087$ at central rapidity ($|\eta| < 1.74$) and 0.09×0.174 to 0.35×0.174 at forward rapidity ($1.74 < |\eta| < 3$).

A silicon tracker is located inside the ECAL. The tracker consists of two main detectors: three barrel layers and two endcap disks per side of silicon pixel detectors, covering the region from 4 cm to 15 cm in radius, and within 49 cm on either side of the nominal collision point along the LHC beam axis; ten barrel layers and twelve endcap disks per side of silicon strip detectors, covering the region from 25 to 110 cm in radius, and within 280 cm on either side of the nominal collision point along the LHC beam axis. The tracker acceptance extends up to a pseudorapidity of $|\eta| = 2.5$. The tracker, ECAL, and HCAL are immersed in a 3.8 T axial magnetic field, which enables the measurement of charged particle momenta over more than four orders of magnitude, from less than 100 MeV to more than 1 TeV, by reconstructing their trajectories as they traverse the inner tracking system. With the silicon tracker, the transverse momentum resolution for high-momentum tracks (100 GeV) is around 1–2% up to $|\eta| = 1.6$; beyond this η value it degrades due to the reduced lever arm.

3 Data and Simulation Samples

The data sample used in this analysis corresponds to a total integrated luminosity of $(35.9 \pm 1.4) \text{ pb}^{-1}$ [20] recorded in 2010 with the CMS detector. The simulated samples were generated with PYTHIA version 6.4.20 [21], the CTEQ6L [22] parton distribution functions (PDFs), and the Z2 parameter set [23]. Generated events are passed through the full GEANT4 [24] simulation of the CMS detector and are then reconstructed using the same algorithm as for the data. For the simulation of the signal and background, two sets of samples generated with PYTHIA are used: one containing direct photons produced in $q\bar{q}$ Compton scattering and $q\bar{q}$ annihilation,

and a second one generated with all $2 \rightarrow 2$ QCD processes that include photons from initial- and final-state radiation (ISR and FSR), photons from parton showers, and photons from neutral meson decays. Isolated direct photons, ISR and FSR photons, and photons from parton showers are treated as signal, while all other photons are considered to be background. In the simulation, a signal photon must have an isolation sum of less than 5 GeV. The isolation sum is calculated as the sum of the E_T of all charged and neutral particles, after removing the photon, within a cone of $R \equiv \sqrt{(\eta - \eta^\gamma)^2 + (\phi - \phi^\gamma)^2} = 0.4$, η^γ and ϕ^γ being the coordinates of the photon. The 5 GeV threshold at the generator level was chosen to ensure greater than 95% efficiency for direct photons and minimise dependence of the efficiency on the variation of underlying event models.

4 Event Selection

Events with high- E_T photons are selected online by a two-level trigger system. At the first level, the E_T sum of two neighbouring ECAL trigger towers, a trigger tower being a 5×5 crystal matrix, is required to be above 8 GeV. The events that satisfy this selection are passed on to the second trigger level, the High Level Trigger (HLT). In the HLT, the energy measured in the crystals is clustered using the same clustering algorithm as for the offline photon reconstruction [25, 26]. The events having at least one reconstructed electromagnetic cluster with an E_T above a programmable threshold (E_T^{HLT}) are accepted. In this analysis, E_T^{HLT} of 20, 30, 50, or 70 GeV are used, depending on the run period. Owing to the increase of the LHC instantaneous luminosity and the limited available trigger bandwidth, different rate-reduction factors were applied to the triggers at 20, 30, and 50 GeV. Only data collected without the application of rate-reduction factors are used, therefore the data samples for events with photons with $E_T < 80$ GeV correspond to smaller effective integrated luminosities, as listed in Table 1. Events not coming from pp collisions, such as those from beam-gas interactions or beam scraping in the transport system near the interaction point, which produce considerable activity in the pixel detector, are removed by requiring a good primary interaction vertex to be reconstructed. Such vertices must have at least three tracks and must be within 24 cm (2 cm) of the nominal centre of the detector along (perpendicular to) the beam axis. The efficiency for reconstructing a primary interaction vertex is greater than 99.5% [27]. In addition, at least 25% of the reconstructed tracks in the event are required to satisfy the quality requirements given in Ref. [28].

Table 1: Effective integrated luminosity for each photon E_T range.

E_T (GeV)	Integrated luminosity (pb^{-1})
25–35	2.4 ± 0.1
35–55	8.2 ± 0.3
55–80	17.6 ± 0.7
> 80	35.9 ± 1.4

5 Photon Reconstruction and Identification

Photon showers deposit their energy in several crystals in the ECAL. The presence of material in front of the calorimeter may result in photon conversions. Because of the strong magnetic field, the energy deposited in ECAL by converted photons can be spread in ϕ . The energy is therefore clustered at the electromagnetic calorimeter level by building a cluster that is ex-

tended in ϕ , thus minimising the cluster containment variations due to electromagnetic interactions in the tracker material. The threshold for crystals to be included in the cluster is approximately 1 GeV in transverse energy. In the barrel region of ECAL, clusters are formed from the energy sum in a rectangular strip of 5 crystals along η and up to 35 crystals in ϕ . In the endcap region of ECAL, clusters comprise one or more contiguous arrays of 5×5 crystals. Endcap cluster positions are extrapolated to the preshower where preshower clusters are built. The total endcap cluster energy is the sum of cluster energies in the endcap crystals and preshower.

Energy corrections are applied to the clusters to take into account the interactions with the material in front of ECAL and shower containment; the corrections are parametrised as a function of cluster size, E_T , and η , and are on average 1% [19]. The corrections include the following steps:

- A compensation of the η dependence of the lateral energy leakage since the axes of the truncated-pyramid shaped barrel crystals make an angle of 3° with respect to the vector from the nominal interaction vertex, in both the η and ϕ projections. This correction is applied only to barrel clusters.
- A correction to compensate for interactions with material in front of ECAL. Since these interactions spread energy mainly in the ϕ direction, this loss can be parametrised as a function of the ratio of the cluster size in ϕ to its size in η .
- A residual correction that is a function of the cluster E_T and η , to compensate for variations along η in the amount of material and the dependence on E_T of the bremsstrahlung and conversion processes.

A photon candidate is built from the energy-corrected cluster, and the photon momentum is calculated with respect to the location of the reconstructed primary interaction vertex. If multiple vertices are reconstructed, the vertex with the largest scalar sum of the transverse momenta of the associated tracks (Σp_T) is selected.

The timing of the ECAL signals is required to be consistent with that of collision products [29]. Topological selection criteria are used to suppress direct interactions in the ECAL APDs [30]. The residual contamination has an effect smaller than 0.2% on the measured cross section over the entire E_T range considered. Contamination from noncollision backgrounds is estimated to be negligible [31].

Photons are required to have a transverse energy $E_T > 25$ GeV since above 25 GeV the trigger efficiency is approximately 100% for both the barrel and the endcap photons (Section 7). The measurements are performed in four photon pseudorapidity intervals: $|\eta| < 0.9$ (central barrel), $0.9 < |\eta| < 1.44$ (outer barrel), $1.57 < |\eta| < 2.1$ (low- η endcaps), and $2.1 < |\eta| < 2.5$ (high- η endcaps). This definition excludes the transition region between the barrel and the endcaps ($1.44 < |\eta| < 1.57$) and the region outside of the tracker coverage ($|\eta| > 2.5$). The central barrel has 1–1.5 X_0 less material in front of the ECAL than the outer barrel, while the low- η endcaps have about 0.5 X_0 more material than the high- η endcaps, which motivates the subdivision of the barrel and the endcaps.

As mentioned in Section 1, the major source of background comes from the decays of hadrons (such as $\pi^0 \rightarrow \gamma\gamma$) and nonisolated photons produced by the fragmentation of quarks or gluons. The photons from hadron decays tend to produce a wider shower profile since hadrons are massive and give a nonzero opening angle between the photon daughters. In addition, both the decay photons and nonisolated fragmentation photons are accompanied by a number of neutral and charged hadrons that deposit energy in the ECAL and HCAL and leave multiple tracks in the tracking system. Based on these differences between signal and background,

several photon identification variables are used in this analysis:

- H/E : the ratio of the energy deposited in the HCAL to the energy deposited in the ECAL inside a cone of $R < 0.15$ centred on the reconstructed photon direction.
- $\sigma_{\eta\eta}$: a modified second moment of the electromagnetic energy cluster about its mean η position. This quantity is computed with logarithmic weights and is defined as

$$\sigma_{\eta\eta}^2 = \frac{\sum_i^{5 \times 5} w_i (\eta_i - \bar{\eta}_{5 \times 5})^2}{\sum_i^{5 \times 5} w_i},$$

$$w_i = \max\left(0, 4.7 + \ln \frac{E_i}{E_{5 \times 5}}\right),$$

where E_i and η_i are the energy and pseudorapidity of the i^{th} crystal within a matrix of 5×5 crystals centred on the cluster seed and $E_{5 \times 5}$ and $\bar{\eta}_{5 \times 5}$ are the energy sum of the matrix and the weighted average of the pseudorapidities of the same group.

- ISO_{TRK} : the sum of the transverse momenta (p_T) of all tracks in a hollow cone $0.04 < R < 0.4$ drawn around the photon direction. The tracks pointing to a rectangular strip of width $|\Delta\eta| = 0.015$ centred around the photon position are removed from the sum in order to recover possible photon conversions. In addition, tracks with a transverse (longitudinal) impact parameter above 0.1 (0.2) cm are not included.
- ISO_{ECAL} : the sum of the E_T in the individual ECAL crystals located in a hollow cone, with an inner radius of 3.5 crystals and an outer radius of $R = 0.4$, drawn around the ECAL cluster. The E_T deposited in a strip of width $|\Delta\eta| = 2.5$ crystals centred on the photon position is subtracted from the sum to exclude possible photon conversions.
- ISO_{HCAL} : the sum of the E_T in the HCAL towers in a hollow cone $0.15 < R < 0.4$ centred on the ECAL cluster.

The signal photons are expected to have smaller values of H/E , $\sigma_{\eta\eta}$, ISO_{TRK} , ISO_{ECAL} , and ISO_{HCAL} compared to the background photons. The selection criteria for the two methods are slightly different and are described in detail in Section 6.

6 Extraction of the Prompt Photon Yield

The following subsections describe the details of extracting the photon yield (N^γ) from the two variables (i) E_T/p_T , the ratio of the E_T measured in the ECAL to the p_T measured in the tracker for converted photons, and (ii) ISO , which is $\text{ISO}_{\text{TRK}} + \text{ISO}_{\text{ECAL}} + \text{ISO}_{\text{HCAL}}$.

The photon conversion method relies on the difference in the shape of the E_T/p_T distributions between the signal and background. For an isolated prompt photon, the sum of the p_T of the conversion tracks is on average the same as the energy deposited in the ECAL, and thus the E_T/p_T distribution peaks around one. For photons produced from the decay of π^0 and η in jets, the p_T measured from the conversion electron pairs does not account for the full amount of energy collected in the calorimeter and the E_T/p_T is, on average, above one.

The isolation method relies on the difference in the shape of the ISO distributions. For a photon signal, only underlying event, pile-up, and detector noise may contribute to the ISO ; the ISO distribution falls off quickly at around 5 GeV. For a photon background from neutral hadron decays, the energy of particles that are produced together with π^0 or η from the parton fragmentation adds a significant amount of activity around the decay photon and widens the ISO distribution.

In each method, one of these variables is chosen as a discriminating observable. A set of preselection criteria is applied to increase the signal fraction of the photon sample; the signal-region selection criteria are listed in Table 2. The number of signal events N^γ is obtained by fitting the distribution of the discriminating observable as the sum of two components: signal and background. The shapes of the component distributions are taken from simulation and are validated by methods based on data.

Table 2: Signal-region and sideband-region preselection criteria for the photon conversion and isolation methods.

Cut	Signal region	Sideband region
Photon conversion method		
H/E	< 0.05	< 0.05
ISO _{TRK} (GeV)	$< (2.0 + 0.001E_T)$	$(2.0 + 0.001E_T) - (5.0 + 0.001E_T)$
ISO _{ECAL} (GeV)	$< (4.2 + 0.003E_T)$	$< (4.2 + 0.003E_T)$
ISO _{HICAL} (GeV)	$< (2.2 + 0.001E_T)$	$< (2.2 + 0.001E_T)$
barrel: $\sigma_{\eta\eta}$	< 0.010	$0.010 - 0.015$
endcap: $\sigma_{\eta\eta}$	< 0.030	$0.030 - 0.045$
Isolation method		
H/E	< 0.05	< 0.05
barrel: $\sigma_{\eta\eta}$	< 0.010	$0.0110 - 0.0115$
endcap: $\sigma_{\eta\eta}$	< 0.028	> 0.038

6.1 Photon conversion method

After applying the signal-region preselection criteria in Table 2, converted photons are reconstructed by combining the information in the ECAL and the tracker. The ECAL clusters, built and corrected as described in Section 5, are used as starting points for an inward conversion track search, using the E_T of subclusters as an initial guess for the electron or positron trajectory [25, 32]. The innermost point of the resulting tracks is assumed to be close to the conversion point and used as seed for outward track search of the other arm of the conversion. The pattern recognition includes the average energy loss for electrons passing through the tracker material. Once all tracks have been found and the track collection cleaned with loose selection criteria, pairs of oppositely charged tracks belonging to the same cluster are considered as possible conversion candidates. A vertex fit imposing the condition that these tracks be parallel at the conversion vertex is required to converge with a χ^2 probability greater than 5×10^{-4} . The latter ensures that only good vertices are retained and random or ill-defined pairs are rejected. Furthermore, since the method is based on the matching between energy-momentum of the conversions, the requirement $E_T/p_T < 3$ is applied.

In each E_T bin, the measured E_T/p_T distribution is fitted using a binned extended maximum likelihood method, with the likelihood defined as

$$-\ln L = (N_s + N_b) - \sum_{i=1}^n N_i \ln(N_s \mathcal{P}_s^i + N_b \mathcal{P}_b^i),$$

where N_s and N_b are the numbers of expected signal and background events, n is the number of bins, N_i is the number of observed photon candidates in the i^{th} bin, and \mathcal{P}_s^i and \mathcal{P}_b^i are the signal and background probability density functions integrated over the i^{th} bin.

Both the signal shape \mathcal{P}_s and the background shape \mathcal{P}_b are extracted from simulations. An alternate background shape is extracted from background-enriched data that are selected by defining a two-dimensional sideband region in the $\sigma_{\eta\eta}$ -Iso_{TRK} plane according to the definitions given in Table 2. In this sideband region, photon candidates satisfy loose but fail tight criteria on $\sigma_{\eta\eta}$ and Iso_{TRK}; the other requirements are the same as those for the signal region. The comparison between the E_T/p_T background distributions obtained from simulation and data and is used to quantify the systematic uncertainty related to the modelling of the background shape. More details are found in Section 8.1.

An example of the fit to data is shown in Fig. 1 and the photon yield N^γ for each E_T and η interval is listed in Table 3. Due to the lack of converted photon candidates at large E_T , photon conversion results are measured for $E_T < 200$ GeV. Figure 2 shows the measured signal purity, defined as the estimated fraction of true prompt photons over all reconstructed photons that satisfy the selection criteria. The signal purity clearly increases with photon transverse energy, as expected from simulation studies.

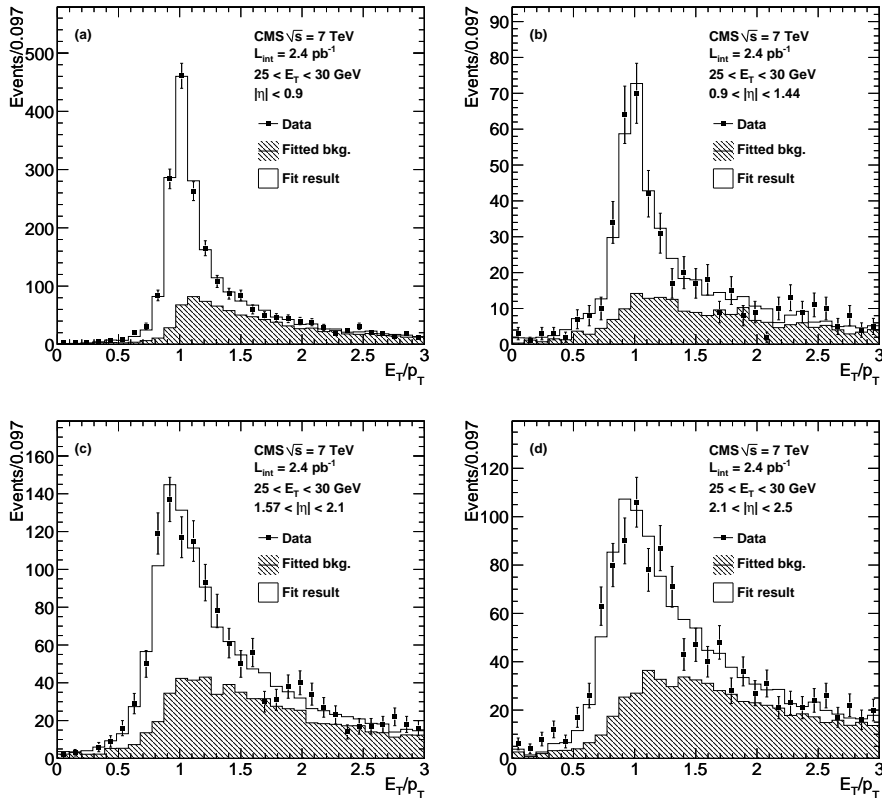


Figure 1: Measured E_T/p_T distributions for converted photon candidates with $E_T = 25\text{--}30$ GeV, in the four η regions considered. The binned extended maximum likelihood fit result (open histogram) is overlaid in each plot. The fitted component from background is shown by hatched histograms.

6.2 Isolation method

Photons are required to satisfy the signal-region preselection criteria listed in Table 2. Background from electrons is suppressed by requiring the absence of a short track segment, built from either two or three hits in the silicon pixel detector, consistent with an electron track matching the observed location and energy of the photon candidate (pixel veto requirement).

Table 3: Measured signal yield N^γ from the photon conversion method. The uncertainty on the yield is the statistical uncertainty from the extended maximum likelihood fit.

E_T (GeV)	$ \eta < 0.9$	$0.9 < \eta < 1.44$	$1.57 < \eta < 2.1$	$2.1 < \eta < 2.5$
25–30	1254 ± 44	275 ± 26	661 ± 43	577 ± 40
30–35	648 ± 31	157 ± 26	280 ± 31	298 ± 29
35–40	1126 ± 40	262 ± 40	618 ± 39	446 ± 36
40–45	711 ± 49	197 ± 21	362 ± 31	268 ± 26
45–50	436 ± 35	115 ± 13	235 ± 40	170 ± 35
50–55	262 ± 27	75 ± 10	183 ± 26	114 ± 18
55–60	444 ± 27	101 ± 8	241 ± 31	142 ± 17
60–65	255 ± 22	56 ± 5	159 ± 15	119 ± 12
65–70	181 ± 13	41 ± 6	104 ± 13	89 ± 8
70–80	254 ± 18	73 ± 9	130 ± 18	93 ± 14
80–100	437 ± 19	98 ± 8	231 ± 26	122 ± 15
100–120	177 ± 7	42 ± 3	61 ± 8	41 ± 5
120–200	134 ± 6	22 ± 2	65 ± 3	22 ± 5

The signal and background component distributions are parametrised with analytic functions. For the signal component, a convolution of exponential and Gaussian functions is used:

$$S(x) = \exp(ax) \otimes \text{Gauss}(\mu, \sigma, x), \quad (1)$$

while for the background the threshold function is used:

$$B(x) = (1 - p_1(x - p_0))^{p_2} \times (1 - e^{p_3(x - p_0)}). \quad (2)$$

Here, x is the ISO variable. Other parametrisations give a much larger χ^2 and fail to describe the observed ISO distributions. Using these parametrisations, an unbinned extended maximum likelihood fit to the measured ISO distribution is performed for the region $-1 < x < 20$ GeV, with the likelihood defined as

$$-\ln L = N_s + N_b - \sum_{i=1}^N \ln(N_s \mathcal{P}_s^i + N_b \mathcal{P}_b^i),$$

where N_s and N_b are the expected signal and background yields, N is the number of observed photon candidates, and \mathcal{P}_s^i and \mathcal{P}_b^i are the signal and background probability density functions evaluated with the ISO of photon candidate i . The signal and background probability density functions are obtained by normalising the integrals of $S(x)$ and $B(x)$ to unity in the fit range, respectively:

$$\mathcal{P}_s^i = \frac{1}{\int_{-1}^{20} S(x) dx} S(x^i),$$

and

$$\mathcal{P}_b^i = \frac{1}{\int_{-1}^{20} B(x) dx} B(x^i),$$

where x^i is the measured ISO of photon candidate i .

While fitting the observed ISO distributions in data, the values of the shape parameters in \mathcal{P}_s and \mathcal{P}_b are not fixed. The two signal shape parameters μ and σ in Eq. (1) and two background

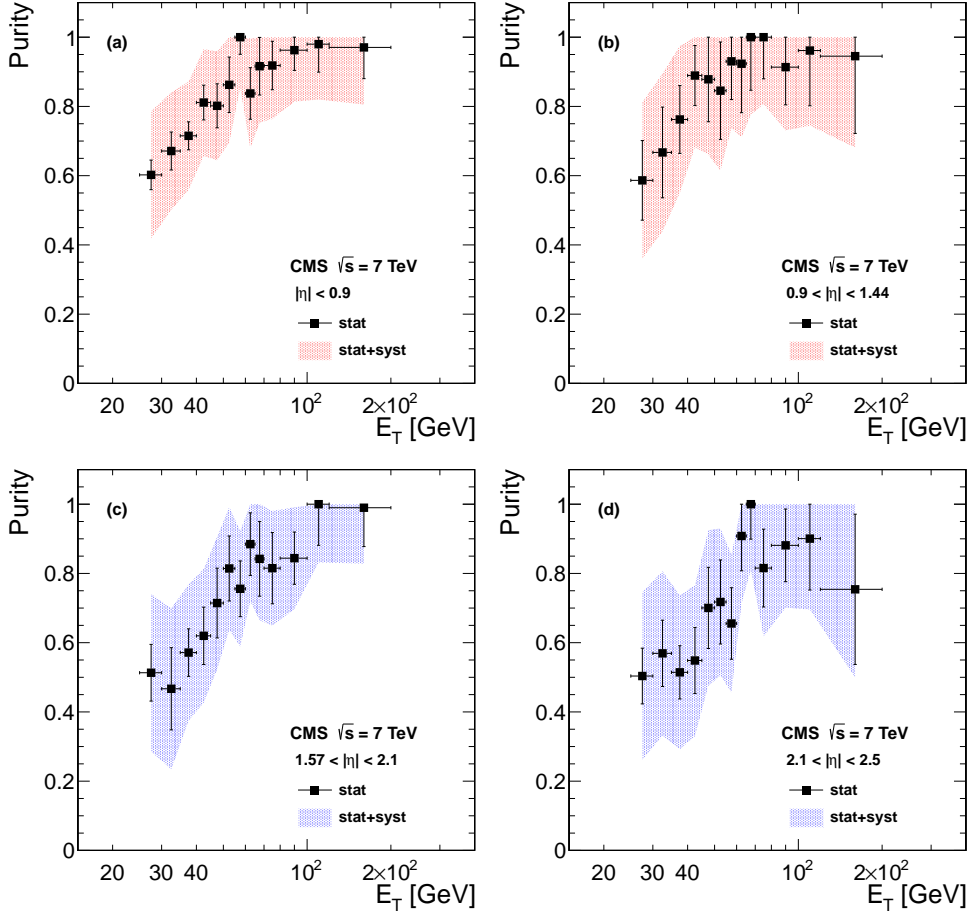


Figure 2: Measured signal purity for $0 < E_T/p_T < 3$ with the photon conversion method in the four η regions. The vertical error bars show the statistical uncertainties, while the shaded areas show the statistical and systematic uncertainties added in quadrature. Estimation of the systematic uncertainties is discussed in Section 8.

shape parameters p_1 and p_2 in Eq. (2) are determined from the fit to data directly, while the exponential tail of the signal a , the background turn-on power p_3 , and the background starting point p_0 are constrained in the fit.

The constrained values of parameter a and parameters p_0 and p_3 are obtained first by fitting the simulated signal events with the parametrisation in Eq. (1) and simulated background events with the parametrisation in Eq. (2), respectively. Then, the constrained values are further corrected with data-to-simulation scaling factors. A difference between data and simulation is observed due to the imperfect modelling of detector noise, the underlying event, pile-up, and the hadronization process.

To derive the scaling factor for the parameter a , low-bremsstrahlung electrons from $Z^0 \rightarrow e^+e^-$ decays are selected as described in Ref. [26]. The amount of bremsstrahlung is obtained from the relative difference between the momentum measured at the last point (p_{out}) on the electron track and the momentum measured at the origin (p_{in}). Here, “low bremsstrahlung” means that the ratio $(p_{\text{in}} - p_{\text{out}}) / p_{\text{in}}$ is less than 0.15. A fit to the electron ISO distribution is performed using the parametrisation in Eq. (1); the ratio of the value of a obtained from electron data to that from electron simulation is taken as the scaling factor for the parameter a of the photon signal shape.

To derive the scaling factors for the parameters p_0 and p_3 , a background-enriched sample is selected with the sideband-region selection criteria listed in Table 2; the contamination of signal in this sideband region is negligible. In this sideband region, photon candidates satisfy the loose but fail the tight criterion on $\sigma_{\eta\eta}$; the other requirements are the same as those for the signal region. Then, fits to the sideband-region ISO distributions in the data and in the simulation, using the parametrisation in Eq. (2), are performed to obtain the scaling factor.

Figure 3 shows the result of the fit for photons with $E_T = 80\text{--}100$ GeV in the four η intervals. The value of ISO may be negative given that an average value is used to subtract the contribution of detector noise in the computation of Iso_{ECAL} and Iso_{HCAL} variables. Table 4 lists the signal yields N^γ for each E_T and η bin. The results for $E_T < 50$ GeV in the endcaps are not used in the measurement due to the large systematic uncertainties in the modelling of the background shape. In order to minimise dependence on the model of isolation, the signal yields are quoted for $\text{ISO} < 5$ GeV. Because the signal and background-enriched samples are small in the highest E_T bin (300–400 GeV), the value of N^γ is obtained by counting the number of observed photon candidates assuming 100% purity, instead of performing the fit. Such an assumption is justified by the fact that purity increases with E_T , as shown in Fig. 4.

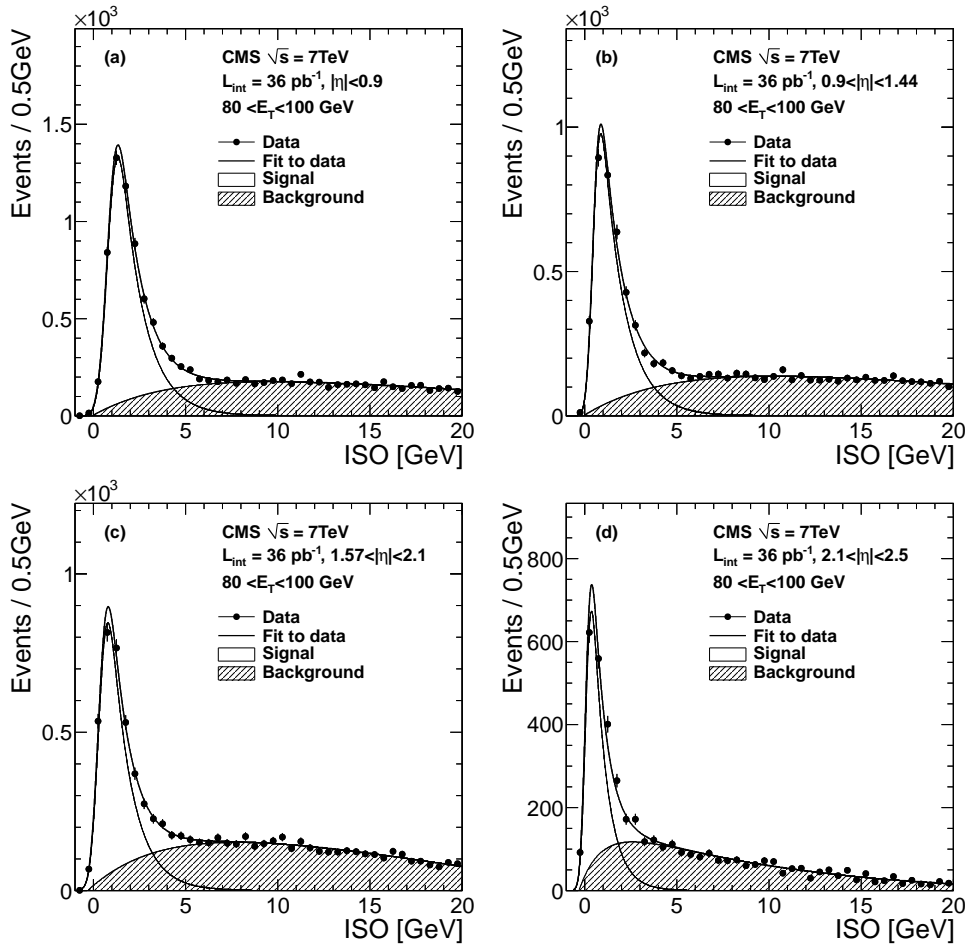


Figure 3: Measured ISO distributions for candidates with $E_T = 80\text{--}100$ GeV. The unbinned maximum likelihood fit result (solid line) is overlaid in each plot. The fitted signal and background components are also shown. Imperfections of the fitting model are included as part of the systematic uncertainties.

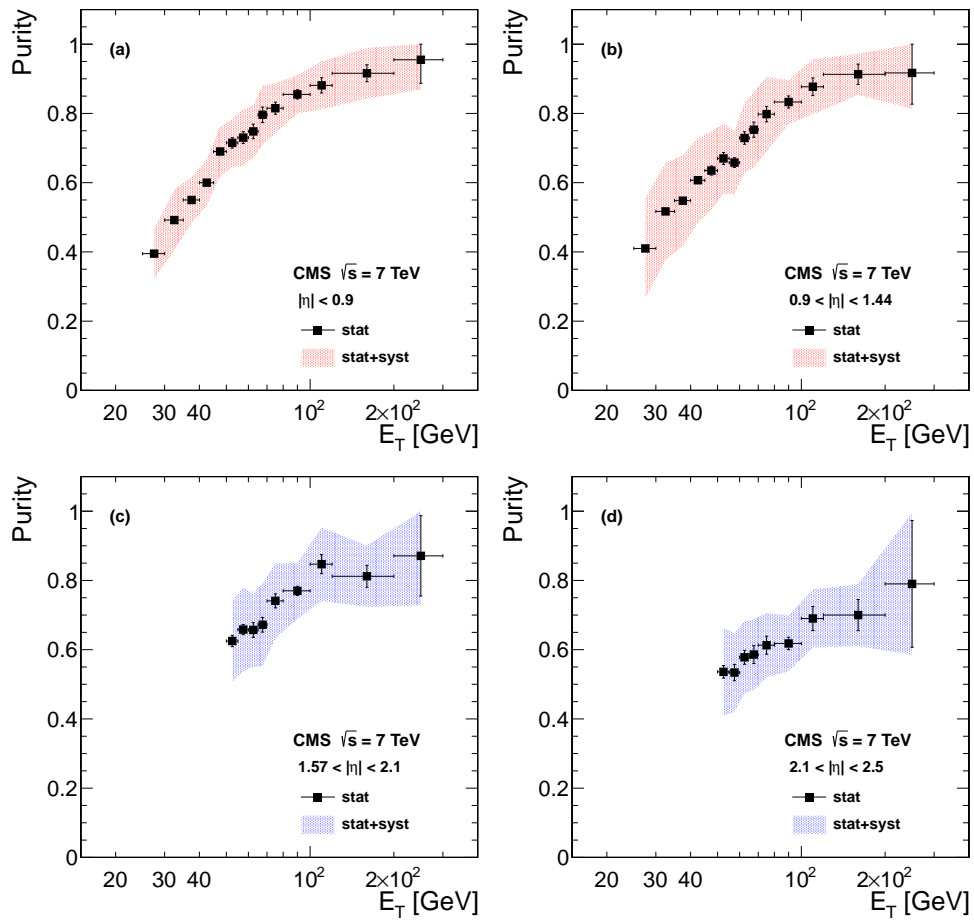


Figure 4: Measured signal purity for $\text{ISO} < 5 \text{ GeV}$ with the isolation method in the four η regions. The purity for the bin $E_T = 300\text{--}400 \text{ GeV}$ is not shown. The vertical error bars show the statistical uncertainties, while the shaded areas show the statistical and systematic uncertainties added in quadrature. Estimation of the systematic uncertainties is discussed in Section 8.

Table 4: Measured signal yield N^γ from the isolation method. The uncertainty on the yield is the statistical uncertainty from the extended maximum likelihood fit.

E_T (GeV)	$ \eta < 0.9$	$0.9 < \eta < 1.44$	$1.57 < \eta < 2.1$	$2.1 < \eta < 2.5$
25–30	15951 ± 209	12088 ± 165	–	–
30–35	8193 ± 151	5977 ± 101	–	–
35–40	14813 ± 179	10384 ± 131	–	–
40–45	8568 ± 121	5790 ± 94	–	–
45–50	5548 ± 92	3425 ± 72	–	–
50–55	3400 ± 71	2138 ± 54	2154 ± 56	1298 ± 44
55–60	4906 ± 115	3067 ± 67	3155 ± 69	1747 ± 77
60–65	3280 ± 92	2143 ± 52	2015 ± 66	1209 ± 42
65–70	2397 ± 67	1521 ± 44	1378 ± 44	822 ± 36
70–80	3013 ± 64	1928 ± 54	1812 ± 50	1042 ± 44
80–100	5487 ± 85	3489 ± 73	3193 ± 54	1679 ± 49
100–120	2128 ± 53	1397 ± 41	1210 ± 39	572 ± 29
120–200	1842 ± 49	1111 ± 36	887 ± 35	396 ± 25
200–300	217 ± 15	121 ± 12	81 ± 11	27 ± 6
300–400	44 ± 7	26 ± 5	8 ± 3	1 ± 1

7 Efficiency Estimation

The selection efficiency can be factorised into several contributions, corresponding to the different steps of the selection process, and can be expressed as

$$\epsilon = \epsilon_{\text{reco}} \times \epsilon_{\text{id1}} \times \epsilon_{\text{trig}} \times \epsilon_{\text{id2}}.$$

The reconstruction efficiency ϵ_{reco} is defined as the ratio of the number of true prompt photons that are reconstructed to the number of true prompt photons that are generated with true E_T and η and have a generator-level isolation less than 5 GeV (Section 3). The value of ϵ_{reco} is 99.8% for all E_T and η bins and is determined from simulated photon signal events.

The preselection efficiency ϵ_{id1} is defined as the ratio of the number of true prompt photons that are reconstructed and satisfy the preselection requirements in Table 2 (with additional requirement of $\text{ISO} < 5$ GeV for the isolation method) to the number of true prompt photons that are reconstructed. The value of ϵ_{id1} is determined from simulated photon signal events first and then multiplied by a data-to-simulation scaling factor. To derive this data-to-simulation scaling factor, a technique called “tag-and-probe” [33] that uses electrons from $Z^0 \rightarrow e^+e^-$ decays is applied. The simulation predicts a few percent difference in the efficiency ϵ_{id1} between photons and electrons; half of this difference is taken as a systematic uncertainty. In addition, the scaling factor is measured in various time periods that correspond to different average numbers of pile-up events due to multiple pp interactions in the same bunch crossing. The envelope of the full variation, approximately 3–5% depending on the selection criteria and photon E_T , is taken as the systematic uncertainty. The derivation of the efficiency scaling factors is described in more detail in Ref. [31].

The trigger efficiency ϵ_{trig} is measured with the tag-and-probe method directly from data and defined with respect to the number of reconstructed electrons satisfying the preselection criteria. The ϵ_{trig} is measured to be $(99.8 \pm 0.1)\%$ for the barrel and $(99.0 \pm 0.7)\%$ for the endcaps.

The symbol ϵ_{id2} represents the efficiency of the pixel veto requirement for the isolation method

while for the photon conversion method it represents the product of three terms: conversion probability, track reconstruction efficiency, and identification efficiency. While ϵ_{id1} and ϵ_{trig} are calibrated with electrons using the “tag-and-probe” technique, ϵ_{id2} must be measured using a different method as described in Sections 7.1 and 7.2.

7.1 Photon conversion method

The tag-and-probe scaling factor on ϵ_{id1} is on average 0.963 ± 0.050 for the barrel and 0.990 ± 0.053 for the endcap. The uncertainty on the scaling factor is dominated by the uncertainty associated with the number of pile-up events, the background estimate underneath the Z^0 mass peak, and the difference between photons and electrons observed in the simulation.

For the photon conversion method, ϵ_{id2} cannot be measured from the $Z^0 \rightarrow e^+e^-$ events and is measured with a different sample. First, a sample is selected in data by applying the H/E and $\sigma_{\eta\eta}$ requirements listed in Table 2. The ISO distribution of these selected candidates is used to extract the yield, N_1 , of signal photons with $\text{ISO} < 5 \text{ GeV}$, using the signal shape from Eq. (1) with the background shape obtained from the simulation. Second, a subsample of these candidates is selected, which, in addition to passing the shower shape selection, also have reconstructed conversion tracks meeting the conversion identification criteria as discussed in Section 6.1. The signal extraction is performed again on the conversion subsample to obtain an estimate of the number of signal photons, N_2 , that converted and passed the conversion identification selection. The ratio between the extracted number of signal events before and after applying the conversion selection, N_2/N_1 , is used as an estimate of the value of ϵ_{id2} .

In simulation, the ϵ_{id2} depends only weakly on the E_T of the photon, but varies strongly with η . Due to the relatively small number of events in the conversion subsample, an average value of the ϵ_{id2} for each η bin is extracted and then corrected for the E_T dependence observed in the simulation. As a cross-check, photon identification criteria and the ISO fit range are varied. The measured ϵ_{id2} is found to be independent of the choice of these parameters.

Figure 5 (a) shows the total efficiency ϵ for the photon conversion method, after taking into account the scaling factors, as a function of photon E_T in the four η regions. The value of ϵ for the photon conversion method is lower than that for the isolation method because of the probability for a photon to convert before reaching the CMS electromagnetic calorimeter and the relatively small conversion reconstruction efficiency. The conversion probability, estimated at the generator level, is between 20% and 70% in the region of $|\eta| < 1.44$ and between 65% and 70% in the region of $1.57 < |\eta| < 2.5$. The efficiency in the region $0.9 < |\eta| < 1.44$ is lower than in the other regions because this region covers the area of transition between the tracker barrel and endcap where the largest amount of material, due to cables and services, is located. This region is especially challenging for electron and conversion reconstruction. Uncertainties on the ϵ_{id1} , ϵ_{id2} , and trigger efficiency ϵ_{trig} are included as sources of systematic uncertainty on the final cross section measurement in Section 8.

7.2 Isolation method

The data-to-simulation scaling factor on ϵ_{id1} measured with the tag-and-probe method varies from 0.971 ± 0.073 to 0.955 ± 0.032 for the barrel and from 0.998 ± 0.056 to 0.990 ± 0.056 for the endcaps, as E_T increases from 20 GeV to 45 GeV.

In addition, as mentioned in Section 6.2, a pixel veto requirement is applied in the isolation method to suppress the contribution of electron background. The efficiency of the pixel veto requirement is estimated with the photons from the final-state radiation of muons in Z^0 decays, i.e. $Z^0 \rightarrow \mu^+\mu^-\gamma$ events. The algorithm used in the pixel veto requirement may be affected by

the presence of nearby muon tracks leading to a false match to the photon. To reduce this bias, events with photons that are close to the muons are removed and the procedure is validated with simulation. A data-to-simulation scaling factor is measured to be 0.996 ± 0.013 for the barrel and 0.959 ± 0.062 for the endcaps.

Figure 5 (b) shows the total efficiency ϵ for the isolation method, after taking into account the scaling factors, as a function of photon E_T in the four η regions. Uncertainties on the ϵ_{id1} , ϵ_{id2} , and trigger efficiency ϵ_{trig} are included as sources of systematic uncertainty on the final cross section measurement in Section 8.

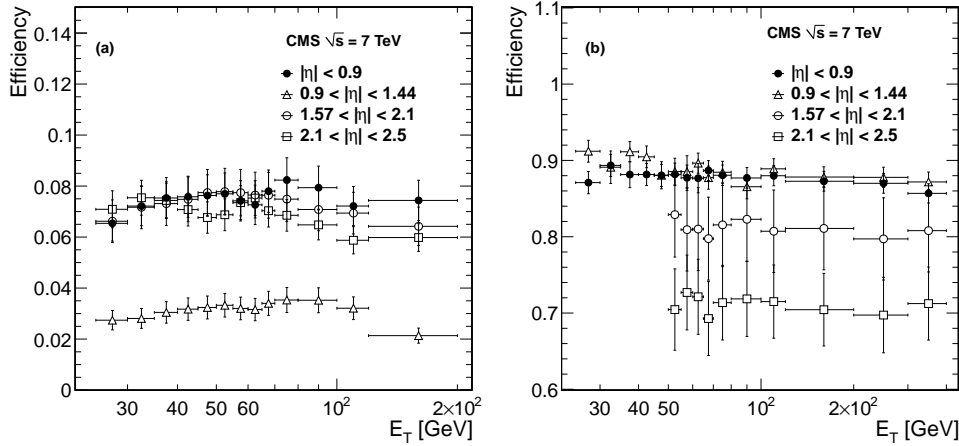


Figure 5: Measured signal efficiency ϵ for the (a) photon conversion and (b) isolation methods in the four η regions. Data-to-simulation scaling factors have been applied. The error bars are dominated by the systematic uncertainties and are 100% correlated between different E_T bins.

8 Systematic Uncertainties

Table 5 summarises the systematic uncertainties on the cross section in the four η regions. The major sources of systematic uncertainties include the uncertainties on the shapes of the signal and background and photon identification efficiency. Sections 8.1 and 8.2 describe the estimation of these dominant systematic uncertainties that are specific to each method.

In addition to the 4% overall uncertainty on the integrated luminosity, uncertainties on the ECAL energy scale and trigger efficiency are 100% correlated between the photon conversion and isolation methods. The uncertainty on the ECAL energy scale is estimated from the Z^0 mass peak positions to be 0.6% for the barrel and 1.5% for the endcaps [34]. The full analysis procedure is repeated by scaling up and down the photon E_T according to the uncertainty, which results in an uncertainty of 4% on the photon cross section. The 4% uncertainty is given by the statistical fluctuations in the yield rather than the expected mean size of the effect. The uncertainty on the trigger efficiency is limited by the available sample of $Z^0 \rightarrow e^+e^-$ events.

For both methods, systematic uncertainties on the signal and background shapes are obtained by pseudo-experiments. The signal or background distribution is varied in the generated pseudo-experiments according to the uncertainty on the shape parameters. The result of each pseudo-experiment is then fitted using the original fit model. The variation of the fitted yield is assigned as the systematic uncertainty. The uncertainties on the efficiency ϵ_{id1} for both methods and ϵ_{id2} for the isolation method are dominated by the limited number of $Z^0 \rightarrow e^+e^-$ and $Z^0 \rightarrow \mu^+\mu^-\gamma$ events available, the pile-up conditions, the background estimate, and the difference between photons and electrons observed in simulation.

The uncertainties due to the bias introduced in the fitting procedure and the amount of electron background result in a less than 6% uncertainty on the measured cross section. The uncertainty due to imperfection of the fitting model is obtained from pseudo-experiments by extracting the difference between observed signal yields and the yields expected under the fitted model. The electron background from $Z^0 \rightarrow e^+e^-$ decays is estimated from the product of the integrated luminosity, the production cross section measured in Ref. [35], and the efficiency from simulated Z^0 events multiplied by a data-to-simulation efficiency scaling factor. The contribution of electron background from $W \rightarrow e\nu$ decays and Drell–Yan processes is estimated following the same procedure. The total contribution of electron background is less than 1% and is taken as a systematic uncertainty.

Table 5: Systematic uncertainties expressed in percent for each source in the four η regions. The ranges, when quoted, indicate the variation over photon E_T . The unfolding correction is discussed in Section 9.

Source	$ \eta < 0.9$	$0.9 < \eta < 1.44$	$1.57 < \eta < 2.1$	$2.1 < \eta < 2.5$
	Common			
Luminosity		4.0		4.0
Energy scale		4.0		4.0
Trigger efficiency		0.1		0.7
	Photon conversion method			
Isolation efficiency	5.2	5.2	5.4	5.4
Conversion efficiency	11	11	8.9	8.9
Fit bias	0–4.1	0–6.1	0.1–4.2	0–5.3
Signal shape	1	2.3	3	3.1
Background shape	0.1–4.8	4.1–5.9	0.3–14	6.2–15
Electron background	0.01–0.1	0.02–0.2	0.05–1.1	0.03–0.8
Unfolding correction	4.0	4.0	4.0	4.0
Total	14–18	14–20	12–21	13–23
	Isolation method			
Efficiency	3.6–7.6	3.6–7.6	8.6	8.6
Fit bias	0.1–2.9	0.1–2.8	0.1–4.0	1.1–4.7
Signal/background shape	1.8–13	1.6–32	4.9–16	7.0–21
N^γ for $E_T = 300\text{--}400$ GeV	4.5	8.3	10	20
Electron background	< 0.1	< 0.1	< 0.1	< 0.1
Unfolding correction	2.0	2.0	2.0	2.0
Total	3.8–18	3.9–35	8.7–18	10–23

8.1 Photon conversion method

A significant source of systematic uncertainty affecting the photon conversion method is the possible mismodelling of the signal and background probability density functions (\mathcal{P}_s and \mathcal{P}_b). To establish the size of this uncertainty, both \mathcal{P}_s and \mathcal{P}_b are checked against the data. For the signal distribution, possible differences in the E_T/p_T distribution are investigated by varying the peak position and the width of the distribution. For each variation, the change in signal yield is computed along with the χ^2 probability of the fit to data. The weighted variance of these varied signal yields is computed using the χ^2 probability for each variation as the weight, and is used to set the systematic uncertainty on the signal shape. For the background, an alternate \mathcal{P}_b is extracted from the observed E_T/p_T distribution in the sideband (background-enriched) region

defined in Table 2. The extraction of the signal yield is repeated using this value of \mathcal{P}_b determined from data, and the size of the difference from the central value is taken as the systematic uncertainty due to background shape. The observed and simulated E_T/p_T distributions in the sideband region are in good agreement and the shapes of E_T/p_T distributions are found to be insensitive to the number of pile-up events in the data.

The systematic uncertainty associated with $\epsilon_{\text{id}2}$ is another significant source of uncertainty. The uncertainty on $\epsilon_{\text{id}2}$ due to the use of the isolation method to extract the numbers of signal candidates N_1 and N_2 (Section 7.1) is estimated in several ways, including a comparison of ISO background shapes from data sideband regions and simulation and a comparison of $\epsilon_{\text{id}2}$ extracted with different photon candidate selections. The statistical uncertainty on the number of candidates used in Section 7.1 to measure the $\epsilon_{\text{id}2}$ from data is also included in the uncertainty. Finally, the $\epsilon_{\text{id}2}$ is recomputed by splitting the data sample into statistically independent halves. The final uncertainty on the $\epsilon_{\text{id}2}$ is chosen to cover the differences seen under each of these variations.

Figure 6 shows the E_T dependence of each dominant systematic uncertainty listed in Table 5 for the photon cross section measured with the photon conversion method. The systematic uncertainty associated with signal/background shape in the η region $|\eta| < 0.9$ increases with photon E_T , which is different from the other η regions for the following reasons. The size of the systematic uncertainty is mainly driven by the difference between the simulated and observed background distributions with sideband selections; it is a balance between the decreasing number of background events at high E_T for this comparison (tending to make the uncertainty larger) and increasing purity (tending to make the uncertainty lower). In this η bin the first effect dominates.

8.2 Isolation method

For the highest- E_T bin in the isolation method (300–400 GeV), the relative systematic uncertainty on N^γ is obtained from the difference between the fitted purity at 200–300 GeV and the assumed 100% purity. For the other E_T bins, the uncertainties associated with the signal and background shapes arise from the uncertainties on the constrained values of the shape parameters a , p_0 , and p_3 in the likelihood fit [Eqs. (1) and (2) in Section 6.2].

The constrained value of the signal parameter a is varied by $\pm 30\%$ to account for the imperfect modelling of pile-up events; the value 30% is the largest data-simulation difference observed among the four η bins in the electron sample. In order to estimate the effect due to the modelling of nondirect photons in PYTHIA, $2 \rightarrow 2$ QCD processes that contain ISR, FSR, and parton shower photons are removed in the signal simulation, which results in a 5% change in the constrained value of parameter a .

The uncertainty on the background shape parameters p_0 and p_3 is mainly driven by the size of background-enriched samples that are selected within the sideband region of $\sigma_{\eta\eta}$ and that are used to derive the data-to-simulation scaling factors. Because of the large statistical uncertainties on the data-to-simulation scaling factors for higher photon E_T bins, the difference between the constrained values obtained by applying and not applying the scaling factors is conservatively included as a systematic uncertainty.

The uncertainty on N^γ from the signal and background shapes is determined from pseudo-experiments by varying simultaneously the values of parameters a , p_0 , and p_3 according to their uncertainties.

Figure 7 shows the E_T dependence of each dominant systematic uncertainty listed in Table 5

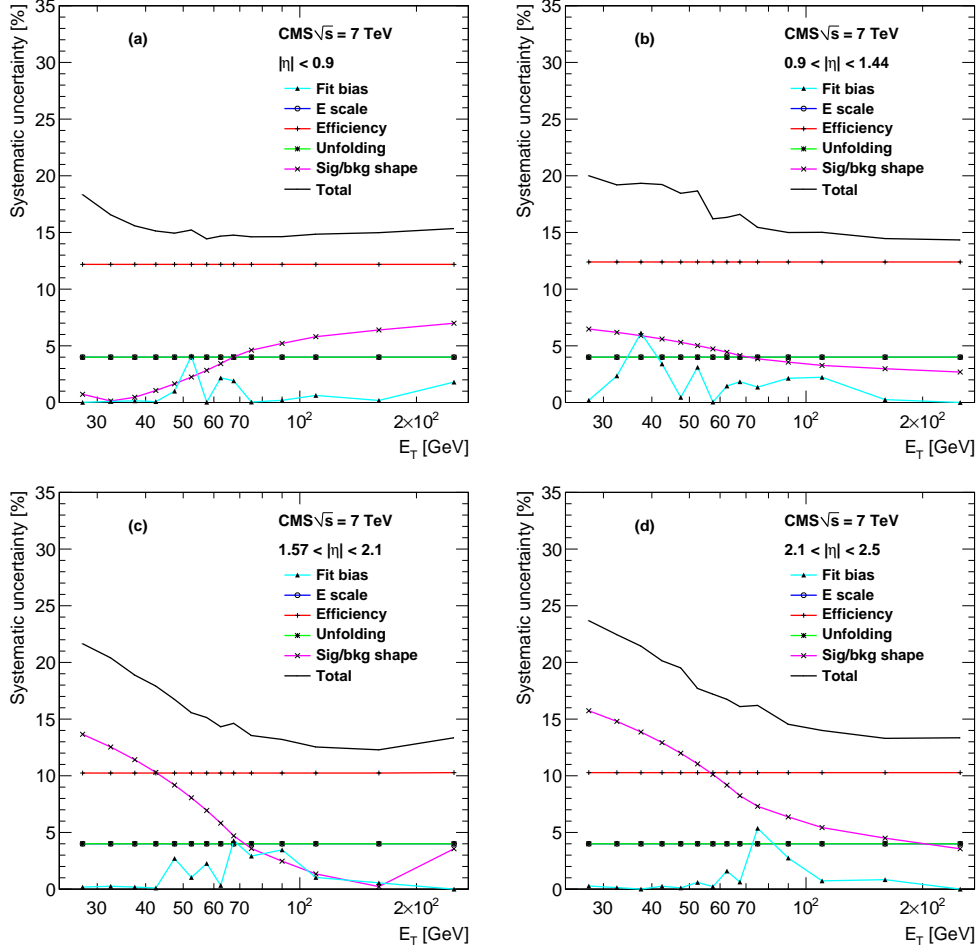


Figure 6: Relative systematic uncertainties on the photon cross section measured with the photon conversion method in the four η regions. Systematic uncertainties due to the uncertainties on the fit bias, energy scale, selection efficiency, unfolding correction factors, and signal and background shapes are shown, as well as their total quadrature sum (upper curve).

for the photon cross section measured with the isolation method. Variations of the systematic uncertainty associated with the signal/background shapes are observed for the following reasons. In general, the uncertainty decreases with photon E_T , which is expected due to the increase of photon purity. However, the difference between simulated and observed ISO distribution increases with E_T . For $E_T < 55$ GeV, only data before the improvement of LHC instantaneous luminosity are used (Table 1) and in this period there are fewer pile-up collisions on average. Therefore, a step or a transition in systematic uncertainty is observed at $E_T = 55$ GeV in Figs. 7 (a) and (b). In addition, due to the lack of high- E_T photon candidates that satisfy side-band selection criteria, a background-enriched sample with photon $E_T = 80$ – 100 GeV is used to derive the data-to-simulation scaling factors for all the E_T bins above 80 GeV. Therefore, for three out of four η regions, a discontinuity in the systematic uncertainty is observed at 100 GeV. The systematic uncertainty on the cross section for low- E_T photons in the outer barrel is larger than in the central barrel because of a larger difference between the simulated and observed isolation distributions.

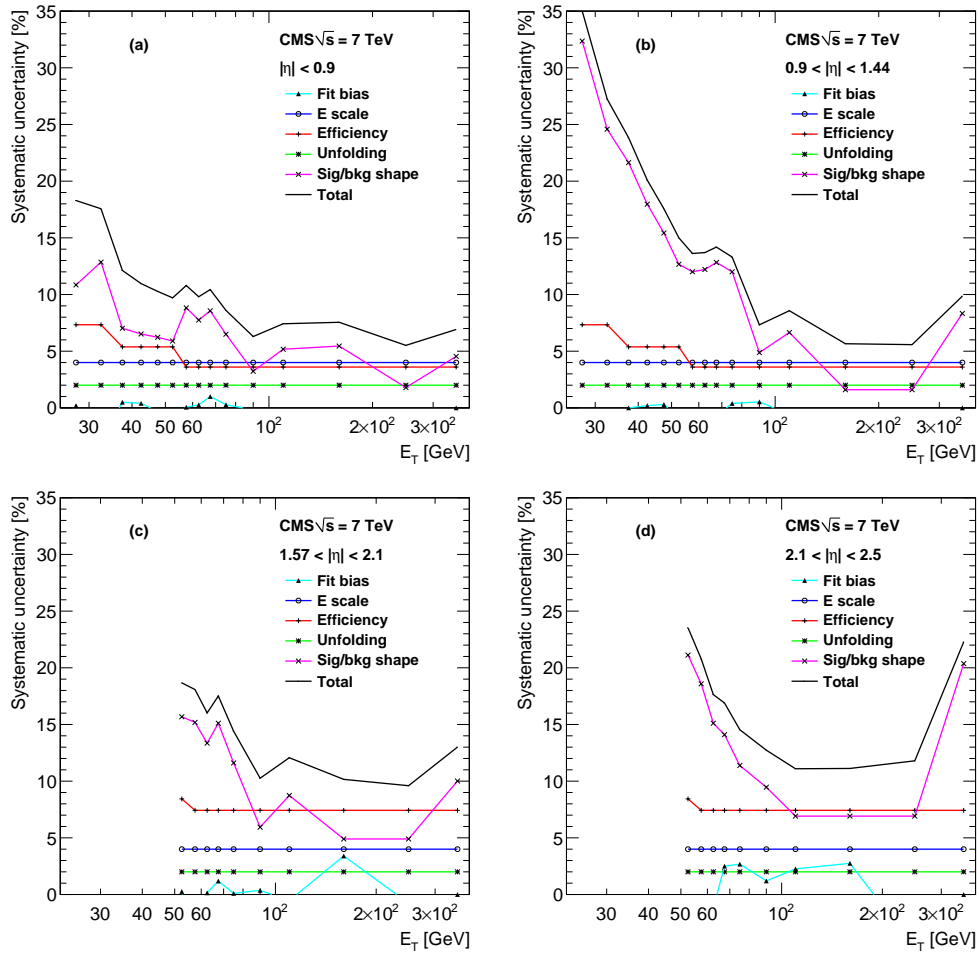


Figure 7: Relative systematic uncertainties on the photon cross section measured with the isolation method in the four η regions. Systematic uncertainties due to the uncertainties on the fit bias, energy scale, selection efficiency, unfolding correction factors, and signal and background shapes are shown, as well as their total quadrature sum (upper curve).

9 Results

The differential cross section is defined as

$$d^2\sigma/dE_T d\eta = N^\gamma \cdot \mathcal{U} / (L \cdot \epsilon \cdot \Delta E_T \cdot \Delta\eta), \quad (3)$$

where N^γ is the signal photon yield measured from data (Section 6), L is the integrated luminosity, \mathcal{U} denotes the bin-by-bin unfolding correction factors, ϵ is the product of the efficiencies (Section 7), and ΔE_T and $\Delta\eta$ are the sizes of the E_T and η bins.

The E_T of a photon candidate can be mismeasured because of detector resolution and imperfections in the reconstruction algorithm. The bin-by-bin unfolding correction \mathcal{U} is applied to account for these effects. The correction is obtained from simulation for each E_T - η bin, by taking the ratio of the generator- to the reconstruction-level photon E_T spectrum. Direct photons, simulated by PYTHIA as described in Section 3, are used to derive the correction. The difference in the correction factors obtained by using the E_T spectrum of direct photons in PYTHIA and by using that of the NLO pQCD predictions [3, 4] is taken as a systematic uncertainty. The resulting relative change on the cross section is listed in Table 5 and shown in Figs. 6 and 7 for the photon conversion and isolation methods, respectively.

After unfolding corrections are applied, the results of the photon conversion and isolation methods are compared for the E_T bins where both are available. The consistency of the results are quantified by the global χ^2 divided by the number of E_T bins; they are 11.8/13, 20.4/13, 12.2/8, and 3.6/8 for the four pseudorapidity intervals, respectively, which indicates a good agreement between the results of the two methods. The results of the two methods are combined using the procedure described in Ref. [36], weighting each method by its corresponding uncertainty in each E_T - η bin. The weights are obtained by inverting the covariance matrix between the two methods, which has elements $C_{ij} = \rho_{ij}\sigma_i\sigma_j$, where σ_i and σ_j are the total uncertainties for the two methods and ρ_{ij} is the correlation coefficient.

Since the value of ρ_{ij} is not known in data, the following procedure is adopted for combining the results. The systematic uncertainties from trigger efficiency and energy scale are fully correlated because the same procedure is applied to both measurements and they give a lower limit on ρ_{ij} . The systematic uncertainties due to signal and background shapes as well as to the fitting bias have negligible correlation, as checked from simulation studies; they provide the upper limit on the correlation coefficients ρ_{ij} . For the remaining sources of uncertainties, the correlation coefficients are varied from zero to one. Each unknown coefficient is varied independently, and for each variation, the resulting value of ρ_{ij} is used in the combination. The final value of the combined cross section is the mean of the central values obtained for each ρ_{ij} . For each value of ρ_{ij} the uncertainty on the combined measurement is evaluated and the final, total uncertainty is conservatively quoted as the mean of the resulting uncertainty distribution plus its standard deviation.

Since the major sources of systematic uncertainties (signal and background shapes) are uncorrelated, the impact on the final combined result of varying the correlations on the remaining sources is limited to the percent level. The central values and uncertainties generated with this procedure were studied in pseudo-experiments to confirm that they have the desired properties.

Since the conversion method has smaller uncertainty than the isolation method at low E_T , it receives a higher weight in the combination at low E_T . The situation is reversed at high E_T . Table 6 lists the final measured cross section with corresponding statistical and systematic uncertainties.

Table 6: Measured isolated prompt photon differential cross section $d^2\sigma/dE_T d\eta$ in the four pseudorapidity regions. The quoted uncertainties are statistical and systematic, respectively.

	$ \eta < 0.9$	$0.9 < \eta < 1.44$
E_T (GeV)	Cross section (nb/GeV)	Cross section (nb/GeV)
25–30	$(7.83 \pm 0.17^{+0.96}_{-0.96}) \times 10^{-1}$	$(6.69 \pm 0.85^{+1.25}_{-1.33}) \times 10^{-1}$
30–35	$(3.85 \pm 0.14^{+0.46}_{-0.42}) \times 10^{-1}$	$(4.07 \pm 0.46^{+0.67}_{-0.55}) \times 10^{-1}$
35–40	$(2.04 \pm 0.04^{+0.19}_{-0.19}) \times 10^{-1}$	$(1.90 \pm 0.19^{+0.31}_{-0.29}) \times 10^{-1}$
40–45	$(1.25 \pm 0.03^{+0.11}_{-0.11}) \times 10^{-1}$	$(1.42 \pm 0.06^{+0.19}_{-0.19}) \times 10^{-1}$
45–50	$(7.93 \pm 0.22^{+0.63}_{-0.66}) \times 10^{-2}$	$(7.81 \pm 0.48^{+0.96}_{-0.93}) \times 10^{-2}$
50–55	$(4.97 \pm 0.16^{+0.37}_{-0.39}) \times 10^{-2}$	$(5.03 \pm 0.24^{+0.54}_{-0.54}) \times 10^{-2}$
55–60	$(3.49 \pm 0.09^{+0.28}_{-0.28}) \times 10^{-2}$	$(3.46 \pm 0.16^{+0.31}_{-0.34}) \times 10^{-2}$
60–65	$(2.31 \pm 0.09^{+0.17}_{-0.18}) \times 10^{-2}$	$(2.18 \pm 0.12^{+0.18}_{-0.22}) \times 10^{-2}$
65–70	$(1.61 \pm 0.07^{+0.12}_{-0.13}) \times 10^{-2}$	$(1.58 \pm 0.10^{+0.14}_{-0.15}) \times 10^{-2}$
70–80	$(1.05 \pm 0.03^{+0.09}_{-0.08}) \times 10^{-2}$	$(1.09 \pm 0.05^{+0.10}_{-0.10}) \times 10^{-2}$
80–100	$(4.80 \pm 0.12^{+0.30}_{-0.28}) \times 10^{-3}$	$(4.86 \pm 0.24^{+0.37}_{-0.35}) \times 10^{-3}$
100–120	$(1.89 \pm 0.05^{+0.14}_{-0.14}) \times 10^{-3}$	$(2.00 \pm 0.10^{+0.21}_{-0.17}) \times 10^{-3}$
120–200	$(4.07 \pm 0.16^{+0.33}_{-0.29}) \times 10^{-4}$	$(4.06 \pm 0.16^{+0.23}_{-0.23}) \times 10^{-4}$
200–300	$(4.00 \pm 0.29^{+0.27}_{-0.27}) \times 10^{-5}$	$(3.60 \pm 0.39^{+0.20}_{-0.20}) \times 10^{-5}$
300–400	$(8.20 \pm 1.22^{+0.59}_{-0.54}) \times 10^{-6}$	$(7.84 \pm 1.53^{+0.75}_{-0.75}) \times 10^{-6}$
	$1.57 < \eta < 2.1$	$2.1 < \eta < 2.5$
E_T (GeV)	Cross section (nb/GeV)	Cross section (nb/GeV)
25–30	$(6.39 \pm 0.50^{+1.35}_{-1.35}) \times 10^{-1}$	$(7.40 \pm 0.58^{+1.74}_{-1.70}) \times 10^{-1}$
30–35	$(2.93 \pm 0.34^{+0.59}_{-0.57}) \times 10^{-1}$	$(4.09 \pm 0.38^{+0.91}_{-0.91}) \times 10^{-1}$
35–40	$(1.92 \pm 0.13^{+0.36}_{-0.36}) \times 10^{-1}$	$(1.97 \pm 0.15^{+0.42}_{-0.41}) \times 10^{-1}$
40–45	$(1.18 \pm 0.10^{+0.20}_{-0.20}) \times 10^{-1}$	$(1.22 \pm 0.12^{+0.24}_{-0.24}) \times 10^{-1}$
45–50	$(7.03 \pm 0.69^{+1.13}_{-1.13}) \times 10^{-2}$	$(8.13 \pm 0.94^{+1.54}_{-1.54}) \times 10^{-2}$
50–55	$(5.63 \pm 0.31^{+0.63}_{-0.58}) \times 10^{-2}$	$(5.34 \pm 0.42^{+0.70}_{-0.65}) \times 10^{-2}$
55–60	$(3.72 \pm 0.21^{+0.42}_{-0.34}) \times 10^{-2}$	$(3.10 \pm 0.22^{+0.39}_{-0.34}) \times 10^{-2}$
60–65	$(2.34 \pm 0.14^{+0.24}_{-0.18}) \times 10^{-2}$	$(2.39 \pm 0.12^{+0.27}_{-0.27}) \times 10^{-2}$
65–70	$(1.61 \pm 0.12^{+0.17}_{-0.13}) \times 10^{-2}$	$(1.75 \pm 0.09^{+0.19}_{-0.18}) \times 10^{-2}$
70–80	$(1.07 \pm 0.06^{+0.10}_{-0.09}) \times 10^{-2}$	$(1.03 \pm 0.05^{+0.11}_{-0.11}) \times 10^{-2}$
80–100	$(4.91 \pm 0.14^{+0.35}_{-0.37}) \times 10^{-3}$	$(3.86 \pm 0.18^{+0.33}_{-0.33}) \times 10^{-3}$
100–120	$(1.48 \pm 0.12^{+0.13}_{-0.07}) \times 10^{-3}$	$(1.39 \pm 0.08^{+0.12}_{-0.12}) \times 10^{-3}$
120–200	$(3.68 \pm 0.16^{+0.27}_{-0.27}) \times 10^{-4}$	$(2.29 \pm 0.19^{+0.18}_{-0.18}) \times 10^{-4}$
200–300	$(2.80 \pm 0.39^{+0.30}_{-0.30}) \times 10^{-5}$	$(1.40 \pm 0.30^{+0.26}_{-0.26}) \times 10^{-5}$
300–400	$(2.80 \pm 0.99^{+0.37}_{-0.34}) \times 10^{-6}$	$(5.42 \pm 5.42^{+1.21}_{-1.21}) \times 10^{-7}$

10 Comparison with Theory

The measured differential cross sections are shown in Fig. 8 for the four pseudorapidity ranges considered, together with NLO pQCD predictions from JETPHOX 1.3.0 [3, 4] using the CT10 PDFs [37] and the BFG set II of fragmentation functions (FFs) [38]. The 4% overall uncertainty on the integrated luminosity is considered separately. The hadronic energy surrounding the photon is required to be at most 5 GeV within $R < 0.4$ at the parton level. The renormalisation, factorisation, and fragmentation scales (μ_R , μ_F , and μ_f) are all set to the E_T of photon. To estimate the effect of the choice of theory scales in the predictions, the three scales are varied independently between $E_T/2$ and $2E_T$ while keeping the ratio of one scale to the other scales, or vice versa, at most two. Retaining the largest cross-section variation at each E_T bin, the predictions change by $\pm 22\%$ to $\pm 7\%$ with increasing E_T . The uncertainty on the predictions due to the PDFs is determined from the 52+1 CT10 PDF sets using the Hessian method [39, 40] with a reduction of a factor of 1.645 to obtain the 68% confidence level (CL) variation. The uncertainty due to the variation of $\alpha_S(M_Z)$ values is estimated from the difference between CT10 PDFs with $\alpha_S(M_Z)$ set to 0.118, and two CT10as sets with $\alpha_S(M_Z)$ set to 0.118 ± 0.001 corresponding to the 68% CL variation. The $\alpha_S(M_Z)$ uncertainty is added in quadrature with the PDF uncertainty [37]; the combined PDF and α_S uncertainties are within the ranges of 2.5–8.0%, 1.6–8.2%, 2.4–8.5%, and 1.7–11% in the four η regions, respectively. Finally, using the BFG set I of FFs instead of the BFG set II yields negligible differences in the predictions.

The theoretical predictions are multiplied by an additional correction factor C to account for the presence of contributions from the underlying event and parton-to-hadron fragmentation, which tend to increase the hadronic energy inside the isolation cone. Using simulated PYTHIA events, C is determined as the ratio between the isolated fraction of the total prompt photon cross section at the hadron level and the same fraction obtained after turning off both multiple-parton interactions (MPI) and hadronization. Four different sets of PYTHIA parameters (Z2 [23], D6T, DWT, and Perugia-0 [41]) are considered. The average of C over all parameter sets, $\bar{C} = 0.975 \pm 0.006$, has little E_T and η dependence. The uncertainty on \bar{C} is the root mean square of the results obtained with the different PYTHIA parameter sets. The correction reduces the predicted cross section, since the presence of extra activity results in some photons failing the isolation requirements.

Overall, predictions from the NLO pQCD calculations agree with the measured cross sections within uncertainties, as shown in Figs. 8 and 9. However, for photons with lower E_T in the η regions $|\eta| < 0.9$, $0.9 < |\eta| < 1.44$, and $1.57 < |\eta| < 2.1$, the cross sections predicted by NLO pQCD tend to be larger than the measured cross sections, similar to the observation in Ref. [15].

11 Conclusion

A measurement of the differential cross section for the production of isolated prompt photons with $E_T = 25\text{--}400$ GeV in pp collisions at $\sqrt{s} = 7$ TeV has been performed in four intervals of pseudorapidity: $|\eta| < 0.9$, $0.9 < |\eta| < 1.44$, $1.57 < |\eta| < 2.1$, and $2.1 < |\eta| < 2.5$. Two variables are explored to estimate the prompt photon yield: the ratio of the energy measured in the electromagnetic calorimeter to the momentum measured in the tracker for converted photons, and the isolation measured in the tracker and calorimeters. The differential cross sections obtained with these two methods are combined into one measurement. Predictions from the NLO pQCD are found to agree with the measured cross section within uncertainties, although at low E_T the predictions tend to be higher than the measured cross section. This measurement probes the kinematic region $0.007 < x_T < 0.114$, extends the previous CMS measurement to

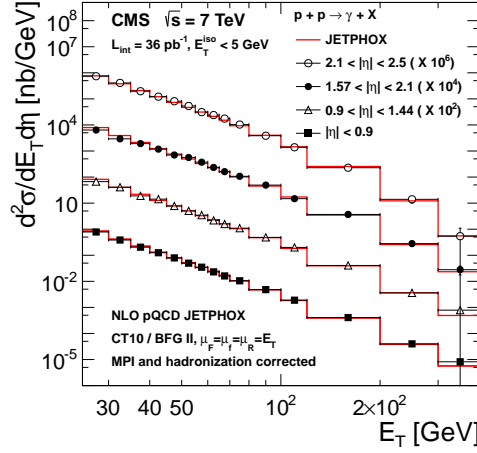


Figure 8: Measured isolated prompt photon differential cross sections (markers) as a function of transverse energy in the four pseudorapidity regions and the predictions from JETPHOX 1.3.0 using the CT10 PDFs (histograms). The error bars are the quadrature sums of statistical and systematic uncertainties on the measurements. The cross sections are scaled by the factors shown in the legend for easier viewing.

wider ranges of photon E_T and pseudorapidity, establishes a benchmark for photon identification and background estimation, and determines the rate of one of the background processes affecting searches for new physics involving photons.

Acknowledgement

We wish to congratulate our colleagues in the CERN accelerator departments for the excellent performance of the LHC machine. We thank the technical and administrative staff at CERN and other CMS institutes. This work was supported by the Austrian Federal Ministry of Science and Research; the Belgium Fonds de la Recherche Scientifique, and Fonds voor Wetenschappelijk Onderzoek; the Brazilian Funding Agencies (CNPq, CAPES, FAPERJ, and FAPESP); the Bulgarian Ministry of Education and Science; CERN; the Chinese Academy of Sciences, Ministry of Science and Technology, and National Natural Science Foundation of China; the Colombian Funding Agency (COLCIENCIAS); the Croatian Ministry of Science, Education and Sport; the Research Promotion Foundation, Cyprus; the Estonian Academy of Sciences and NICPB; the Academy of Finland, Finnish Ministry of Education and Culture, and Helsinki Institute of Physics; the Institut National de Physique Nucléaire et de Physique des Particules / CNRS, and Commissariat à l'Énergie Atomique et aux Énergies Alternatives / CEA, France; the Bundesministerium für Bildung und Forschung, Deutsche Forschungsgemeinschaft, and Helmholtz-Gemeinschaft Deutscher Forschungszentren, Germany; the General Secretariat for Research and Technology, Greece; the National Scientific Research Foundation, and National Office for Research and Technology, Hungary; the Department of Atomic Energy and the Department of Science and Technology, India; the Institute for Studies in Theoretical Physics and Mathematics, Iran; the Science Foundation, Ireland; the Istituto Nazionale di Fisica Nucleare, Italy; the Korean Ministry of Education, Science and Technology and the World Class University program of NRF, Korea; the Lithuanian Academy of Sciences; the Mexican Funding Agencies (CINVESTAV, CONACYT, SEP, and UASLP-FAI); the Ministry of Science and Innovation, New Zealand; the Pakistan Atomic Energy Commission; the State Commission for Scientific Research, Poland; the Fundação para a Ciência e a Tecnologia, Portugal; JINR (Armenia, Belarus, Georgia, Ukraine, Uzbekistan); the Ministry of Science and Technologies of the Russian Feder-

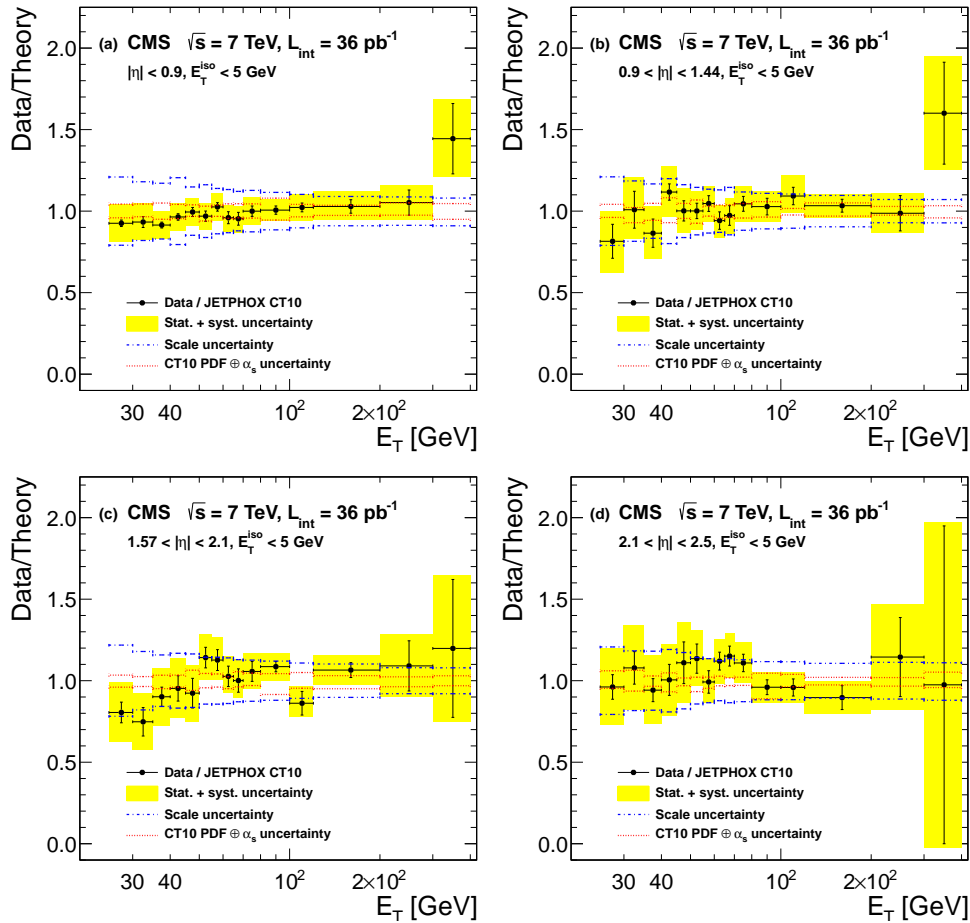


Figure 9: Ratios of the measured isolated prompt photon differential cross section to the NLO pQCD predictions from JETPHOX 1.3.0 using the CT10 PDFs. The vertical error bars show the statistical uncertainties, while the shaded areas show the statistical and systematic uncertainties added in quadrature. The 4% luminosity uncertainty on the data is not included. The two sets of curves show the uncertainties on the theoretical predictions due to their dependence on the renormalisation, factorisation, and fragmentation scales, and on the variation of CT10 α_s and PDFs. A correction to account for extra activity ($\bar{C} = 0.975 \pm 0.006$) is applied to the theoretical predictions, as explained in the text.

ation, the Russian Ministry of Atomic Energy and the Russian Foundation for Basic Research; the Ministry of Science and Technological Development of Serbia; the Ministerio de Ciencia e Innovación, and Programa Consolider-Ingenio 2010, Spain; the Swiss Funding Agencies (ETH Board, ETH Zurich, PSI, SNF, UniZH, Canton Zurich, and SER); the National Science Council, Taipei; the Scientific and Technical Research Council of Turkey, and Turkish Atomic Energy Authority; the Science and Technology Facilities Council, UK; the US Department of Energy, and the US National Science Foundation.

Individuals have received support from the Marie-Curie programme and the European Research Council (European Union); the Leventis Foundation; the A. P. Sloan Foundation; the Alexander von Humboldt Foundation; the Associazione per lo Sviluppo Scientifico e Tecnologico del Piemonte (Italy); the Belgian Federal Science Policy Office; the Fonds pour la Formation à la Recherche dans l'Industrie et dans l'Agriculture (FRIA-Belgium); the Agentschap voor Innovatie door Wetenschap en Technologie (IWT-Belgium); and the Council of Science and Industrial Research, India.

References

- [1] P. Aurenche, R. Baier, M. Fontannaz et al., “The Gluon Contents of the Nucleon Probed with Real and Virtual Photons”, *Phys. Rev. D* **39** (1989) 3275. doi:10.1103/PhysRevD.39.3275.
- [2] H. Baer, J. Ohnemus, and J. F. Owens, “A Next-to-leading Logarithm Calculation of Direct Photon Production”, *Phys. Rev. D* **42** (1990) 61–71. doi:10.1103/PhysRevD.42.61.
- [3] S. Catani, M. Fontannaz, J. P. Guillet et al., “Cross section of isolated prompt photons in hadron-hadron collisions”, *JHEP* **05** (2002) 028, arXiv:hep-ph/0204023. doi:10.1088/1126-6708/2002/05/028.
- [4] P. Aurenche, M. Fontannaz, J.-P. Guillet et al., “A New critical study of photon production in hadronic collisions”, *Phys. Rev. D* **73** (2006) 094007, arXiv:hep-ph/0602133. doi:10.1103/PhysRevD.73.094007.
- [5] PHENIX Collaboration, B. Sahlmueller, “Photons at PHENIX”, in *Proceedings of the 4th international workshop High-pT physics at LHC 09*, p. 035. Prague, 2009. arXiv:0904.4764. PoS(High-pT physics09)035.
- [6] CMS Collaboration, “CMS Physics Technical Design Report, Volume II: Physics Performance”, *J. Phys. G* **34** (2007) 995. doi:10.1088/0954-3899/34/6/S01.
- [7] L. Evans and P. Bryant, “LHC Machine”, *JINST* **3** (2008) S08001. doi:10.1088/1748-0221/3/08/S08001.
- [8] PHENIX Collaboration Collaboration, “Measurement of direct photon production in p + p collisions at $s^{*1/2} = 200\text{-GeV}$ ”, *Phys. Rev. Lett.* **98** (2007) 012002, arXiv:hep-ex/0609031. doi:10.1103/PhysRevLett.98.012002.
- [9] M. Diakonou et al., “Direct production of high pT single photons in pp collisions at the CERN ISR”, *Phys. Lett. B* **87** (1979) 292. doi:10.1016/0370-2693(79)90985-7.
- [10] T. Ferbel and W. R. Molzon, “Direct-photon production in high-energy collisions”, *Rev. Mod. Phys.* **56** (1984) 181. doi:10.1103/RevModPhys.56.181.
- [11] UA2 Collaboration, “Direct photon production at the CERN pbar-p collider”, *Phys. Lett. B* **176** (1986) 239. doi:10.1016/0370-2693(86)90957-3.
- [12] D0 Collaboration, “Measurement of the isolated photon cross section in $p\bar{p}$ collisions at $\sqrt{s} = 1.96\text{ TeV}$ ”, *Phys. Lett. B* **639** (2006) 151, arXiv:hep-ex/0511054. doi:10.1016/j.physletb.2006.04.048.
- [13] CDF Collaboration, “Measurement of the inclusive isolated prompt photon cross section in $p\bar{p}$ collisions at $\sqrt{s} = 1.96\text{ TeV}$ using the CDF Detector”, *Phys. Rev. D* **80** (2009) 111106, arXiv:0910.3623. doi:10.1103/PhysRevD.80.111106.
- [14] CMS Collaboration, “Measurement of the Isolated Prompt Photon Production Cross Section in pp Collisions at $\sqrt{s} = 7\text{ TeV}$ ”, *Phys. Rev. Lett.* **106** (2011) 082001. doi:10.1103/PhysRevLett.106.082001.
- [15] ATLAS Collaboration, “Measurement of the inclusive isolated prompt photon cross section in pp collisions at $\sqrt{s} = 7\text{ TeV}$ with the ATLAS detector”, *Phys. Rev. D* **83** (2011) 052005, arXiv:1012.4389. doi:10.1103/PhysRevD.83.052005.

- [16] ATLAS Collaboration, “Measurement of the inclusive isolated prompt photon cross-section in pp collisions at $\sqrt{s}=7$ TeV using 35 pb^{-1} of ATLAS data”, (2011). arXiv:1108.0253.
- [17] CMS Collaboration, “The CMS experiment at the CERN LHC”, *JINST* **3** (2008) S08004. doi:10.1088/1748-0221/3/08/S08004.
- [18] P. Adzic et al., “Energy resolution of the barrel of the CMS electromagnetic calorimeter”, *JINST* **2** (2007) P04004. doi:10.1088/1748-0221/2/04/P04004.
- [19] CMS Collaboration, “Electromagnetic calorimeter calibration with 7 TeV data”, CMS Physics Analysis Summary CMS-PAS-EGM-10-003, (2010).
- [20] CMS Collaboration, “Absolute luminosity normalization”, CMS Detector Performance Summary CMS-DP-2011-002, (2011).
- [21] T. Sjöstrand, S. Mrenna, and P. Z. Skands, “PYTHIA 6.4 Physics and Manual”, *JHEP* **05** (2006) 026, arXiv:hep-ph/0603175. doi:10.1088/1126-6708/2006/05/026.
- [22] J. Pumplin, D. R. Stump, J. Huston et al., “New Generation of Parton Distributions with Uncertainties from Global QCD analysis”, *JHEP* **07** (2002) 012, arXiv:hep-ph/0201195. doi:10.1088/1126-6708/2002/07/012.
- [23] R. Field, “Early LHC Underlying Event Data - Findings and Surprises”, in *Proceedings of the Hadron Collider Physics Symposium 2010*. 2010. arXiv:1010.3558.
- [24] GEANT 4 Collaboration, “GEANT 4—a simulation toolkit”, *Nucl. Instr. Meth. A* **506** (2003) 250. doi:10.1016/S0168-9002(03)01368-8.
- [25] CMS Collaboration, “Photon reconstruction and identification at $\sqrt{s}=7$ TeV”, CMS Physics Analysis Summary CMS-PAS-EGM-10-005, (2010).
- [26] CMS Collaboration, “Electron reconstruction and identification at $\sqrt{s}=7$ TeV”, CMS Physics Analysis Summary CMS-PAS-EGM-10-004, (2010).
- [27] CMS Collaboration, “Tracking and Primary Vertex Results in First 7 TeV Collisions”, CMS Physics Analysis Summary CMS-PAS-TRK-10-005, (2010).
- [28] CMS Collaboration, “CMS Tracking Performance Results from Early LHC Operation”, *Eur. Phys. J. C* **70** (2010) 1165–1192. doi:10.1140/epjc/s10052-010-1491-3.
- [29] CMS Collaboration, “Time Reconstruction and Performance of the CMS Electromagnetic Calorimeter”, *JINST* **5** (2010) T03011. doi:10.1088/1748-0221/5/03/T03011.
- [30] CMS Collaboration, “Electromagnetic calorimeter commissioning and first results with 7 TeV data”, CMS Note CMS-NOTE-2010-012, (2010).
- [31] CMS Collaboration, “Isolated Photon Reconstruction and Identification at $\sqrt{s}=7$ TeV”, CMS Physics Analysis Summary CMS-PAS-EGM-10-006, (2010).
- [32] N. Marinelli, “Track finding and identification of converted photons”, CMS Note CMS-NOTE-2006-005, (2006).
- [33] CMS Collaboration, “Measuring electron efficiencies at CMS with early data”, CMS Note CMS-NOTE-EGM-07-001, (2007).

-
- [34] CMS Collaboration, "ECAL 2010 performance results", CMS Detector Performance Summary CMS-DPS-2011-008, (2011).
- [35] CMS Collaboration, "Measurements of Inclusive W and Z Cross Sections in pp Collisions at $\sqrt{s}=7$ TeV", *JHEP* **01** (2011) 080. doi:10.1007/JHEP01(2011)080.
- [36] L. Lyons, D. Gibaut, and P. Clifford, "How to Combine Correlated Estimates of a Single Physical Quantity", *Nucl. Instrum. Meth. A* **270** (1988) 110. doi:10.1016/0168-9002(88)90018-6.
- [37] H.-L. Lai, M. Guzzi, J. Huston et al., "New parton distributions for collider physics", *Phys. Rev. D* **82** (2010) 074024, arXiv:1007.2241. doi:10.1103/PhysRevD.82.074024.
- [38] L. Bourhis, M. Fontannaz, and J. P. Guillet, "Quark and gluon fragmentation functions into photons", *Eur. Phys. J. C* **2** (1998) 529, arXiv:hep-ph/9704447. doi:10.1007/s100520050158.
- [39] J. Pumplin et al., "Uncertainties of predictions from parton distribution functions. 2. The Hessian method", *Phys. Rev. D* **65** (2001) 014013, arXiv:hep-ph/0101032. doi:10.1103/PhysRevD.65.014013.
- [40] S. Alekhin et al., "The PDF4LHC Working Group Interim Report", (2011). arXiv:1101.0536.
- [41] P. Z. Skands, "The Perugia Tunes", in *Proceedings of the 1st International Workshop on Multiple Partonic Interactions at the LHC*, p. 284. 2009. arXiv:1003.4220v1.

A The CMS Collaboration

Yerevan Physics Institute, Yerevan, Armenia

S. Chatrchyan, V. Khachatryan, A.M. Sirunyan, A. Tumasyan

Institut für Hochenergiephysik der OeAW, Wien, Austria

W. Adam, T. Bergauer, M. Dragicevic, J. Erö, C. Fabjan, M. Friedl, R. Frühwirth, V.M. Ghete, J. Hammer¹, S. Häsnel, M. Hoch, N. Hörmann, J. Hrubec, M. Jeitler, W. Kiesenhofer, M. Krammer, D. Liko, I. Mikulec, M. Pernicka, B. Rahbaran, H. Rohringer, R. Schöfbeck, J. Strauss, A. Taurok, F. Teischinger, C. Trauner, P. Wagner, W. Waltenberger, G. Walzel, E. Widl, C.-E. Wulz

National Centre for Particle and High Energy Physics, Minsk, Belarus

V. Mossolov, N. Shumeiko, J. Suarez Gonzalez

Universiteit Antwerpen, Antwerpen, Belgium

S. Bansal, L. Benucci, E.A. De Wolf, X. Janssen, S. Luyckx, T. Maes, L. Mucibello, S. Ochesanu, B. Roland, R. Rougny, M. Selvaggi, H. Van Haevermaet, P. Van Mechelen, N. Van Remortel

Vrije Universiteit Brussel, Brussel, Belgium

F. Blekman, S. Blyweert, J. D'Hondt, R. Gonzalez Suarez, A. Kalogeropoulos, M. Maes, A. Olbrechts, W. Van Doninck, P. Van Mulders, G.P. Van Onsem, I. Vilella

Université Libre de Bruxelles, Bruxelles, Belgium

O. Charaf, B. Clerbaux, G. De Lentdecker, V. Dero, A.P.R. Gay, G.H. Hammad, T. Hreus, P.E. Marage, A. Raval, L. Thomas, G. Vander Marcken, C. Vander Velde, P. Vanlaer

Ghent University, Ghent, Belgium

V. Adler, A. Cimmino, S. Costantini, M. Grunewald, B. Klein, J. Lellouch, A. Marinov, J. Mccartin, D. Ryckbosch, F. Thyssen, M. Tytgat, L. Vanelderen, P. Verwilligen, S. Walsh, N. Zaganidis

Université Catholique de Louvain, Louvain-la-Neuve, Belgium

S. Basegmez, G. Bruno, J. Caudron, L. Ceard, E. Cortina Gil, J. De Favereau De Jeneret, C. Delaere, D. Favart, A. Giammanco, G. Grégoire, J. Hollar, V. Lemaitre, J. Liao, O. Militaru, C. Nuttens, S. Owyn, D. Pagano, A. Pin, K. Piotrkowski, N. Schul

Université de Mons, Mons, Belgium

N. Bely, T. Caebergs, E. Daubie

Centro Brasileiro de Pesquisas Fisicas, Rio de Janeiro, Brazil

G.A. Alves, L. Brito, D. De Jesus Damiao, M.E. Pol, M.H.G. Souza

Universidade do Estado do Rio de Janeiro, Rio de Janeiro, Brazil

W.L. Aldá Júnior, W. Carvalho, E.M. Da Costa, C. De Oliveira Martins, S. Fonseca De Souza, D. Matos Figueiredo, L. Mundim, H. Nogima, V. Oguri, W.L. Prado Da Silva, A. Santoro, S.M. Silva Do Amaral, A. Sznajder

Instituto de Fisica Teorica, Universidade Estadual Paulista, Sao Paulo, Brazil

C.A. Bernardes², F.A. Dias³, T. Dos Anjos Costa², T.R. Fernandez Perez Tomei, E. M. Gregores², C. Lagana, F. Marinho, P.G. Mercadante², S.F. Novaes, Sandra S. Padula

Institute for Nuclear Research and Nuclear Energy, Sofia, Bulgaria

N. Darmenov¹, V. Genchev¹, P. Iaydjiev¹, S. Piperov, M. Rodozov, S. Stoykova, G. Sultanov, V. Tcholakov, R. Trayanov, M. Vutova

University of Sofia, Sofia, Bulgaria

A. Dimitrov, R. Hadjiiska, A. Karadzhinova, V. Kozhuharov, L. Litov, M. Mateev, B. Pavlov, P. Petkov

Institute of High Energy Physics, Beijing, China

J.G. Bian, G.M. Chen, H.S. Chen, C.H. Jiang, D. Liang, S. Liang, X. Meng, J. Tao, J. Wang, J. Wang, X. Wang, Z. Wang, H. Xiao, M. Xu, J. Zang, Z. Zhang

State Key Lab. of Nucl. Phys. and Tech., Peking University, Beijing, China

Y. Ban, S. Guo, Y. Guo, W. Li, Y. Mao, S.J. Qian, H. Teng, B. Zhu, W. Zou

Universidad de Los Andes, Bogota, Colombia

A. Cabrera, B. Gomez Moreno, A.A. Ocampo Rios, A.F. Osorio Oliveros, J.C. Sanabria

Technical University of Split, Split, Croatia

N. Godinovic, D. Lelas, K. Lelas, R. Plestina⁴, D. Polic, I. Puljak

University of Split, Split, Croatia

Z. Antunovic, M. Dzelalija, M. Kovac

Institute Rudjer Boskovic, Zagreb, Croatia

V. Brigljevic, S. Duric, K. Kadija, J. Luetic, S. Morovic

University of Cyprus, Nicosia, Cyprus

A. Attikis, M. Galanti, J. Mousa, C. Nicolaou, F. Ptochos, P.A. Razis

Charles University, Prague, Czech Republic

M. Finger, M. Finger Jr.

Academy of Scientific Research and Technology of the Arab Republic of Egypt, Egyptian Network of High Energy Physics, Cairo, Egypt

Y. Assran⁵, A. Ellithi Kamel, S. Khalil⁶, M.A. Mahmoud⁷, A. Radi⁸

National Institute of Chemical Physics and Biophysics, Tallinn, Estonia

A. Hektor, M. Kadastik, M. Müntel, M. Raidal, L. Rebane, A. Tiko

Department of Physics, University of Helsinki, Helsinki, Finland

V. Azzolini, P. Eerola, G. Fedi, M. Voutilainen

Helsinki Institute of Physics, Helsinki, Finland

S. Czellar, J. Härkönen, A. Heikkinen, V. Karimäki, R. Kinnunen, M.J. Kortelainen, T. Lampén, K. Lassila-Perini, S. Lehti, T. Lindén, P. Luukka, T. Mäenpää, E. Tuominen, J. Tuominiemi, E. Tuovinen, D. Ungaro, L. Wendland

Lappeenranta University of Technology, Lappeenranta, Finland

K. Banzuzi, A. Karjalainen, A. Korpela, T. Tuuva

Laboratoire d'Annecy-le-Vieux de Physique des Particules, IN2P3-CNRS, Annecy-le-Vieux, France

D. Sillou

DSM/IRFU, CEA/Saclay, Gif-sur-Yvette, France

M. Besancon, S. Choudhury, M. Dejardin, D. Denegri, B. Fabbro, J.L. Faure, F. Ferri, S. Ganjour, F.X. Gentit, A. Givernaud, P. Gras, G. Hamel de Monchenault, P. Jarry, E. Locci, J. Malcles, M. Marionneau, L. Millischer, J. Rander, A. Rosowsky, I. Shreyber, M. Titov, P. Verrecchia

Laboratoire Leprince-Ringuet, Ecole Polytechnique, IN2P3-CNRS, Palaiseau, France

S. Baffioni, F. Beaudette, L. Benhabib, L. Bianchini, M. Bluj⁹, C. Broutin, P. Busson, C. Charlot, T. Dahms, L. Dobrzynski, S. Elgammal, R. Granier de Cassagnac, M. Haguenaer, P. Miné, C. Mironov, C. Ochando, P. Paganini, D. Sabes, R. Salerno, Y. Sirois, C. Thiebaut, B. Wyslouch¹⁰, A. Zabi

Institut Pluridisciplinaire Hubert Curien, Université de Strasbourg, Université de Haute Alsace Mulhouse, CNRS/IN2P3, Strasbourg, France

J.-L. Agram¹¹, J. Andrea, D. Bloch, D. Bodin, J.-M. Brom, M. Cardaci, E.C. Chabert, C. Collard, E. Conte¹¹, F. Drouhin¹¹, C. Ferro, J.-C. Fontaine¹¹, D. Gelé, U. Goerlach, S. Greder, P. Juillot, M. Karim¹¹, A.-C. Le Bihan, Y. Mikami, P. Van Hove

Centre de Calcul de l'Institut National de Physique Nucleaire et de Physique des Particules (IN2P3), Villeurbanne, France

F. Fassi, D. Mercier

Université de Lyon, Université Claude Bernard Lyon 1, CNRS-IN2P3, Institut de Physique Nucléaire de Lyon, Villeurbanne, France

C. Baty, S. Beauceron, N. Beaupere, M. Bedjidian, O. Bondu, G. Boudoul, D. Boumediene, H. Brun, J. Chasserat, R. Chierici, D. Contardo, P. Depasse, H. El Mamouni, J. Fay, S. Gascon, B. Ille, T. Kurca, T. Le Grand, M. Lethuillier, L. Mirabito, S. Perries, V. Sordini, S. Tosi, Y. Tschudi, P. Verdier, S. Viret

Institute of High Energy Physics and Informatization, Tbilisi State University, Tbilisi, Georgia

D. Lomidze

RWTH Aachen University, I. Physikalisches Institut, Aachen, Germany

G. Anagnostou, S. Beranek, M. Edelhoff, L. Feld, N. Heracleous, O. Hindrichs, R. Jussen, K. Klein, J. Merz, N. Mohr, A. Ostapchuk, A. Perieanu, F. Raupach, J. Sammet, S. Schael, D. Sprenger, H. Weber, M. Weber, B. Wittmer

RWTH Aachen University, III. Physikalisches Institut A, Aachen, Germany

M. Ata, E. Dietz-Laursonn, M. Erdmann, T. Hebbeker, C. Heidemann, A. Hinzmann, K. Hoepfner, T. Klimkovich, D. Klingebiel, P. Kreuzer, D. Lanske[†], J. Lingemann, C. Magass, M. Merschmeyer, A. Meyer, P. Papacz, H. Pieta, H. Reithler, S.A. Schmitz, L. Sonnenschein, J. Steggemann, D. Teyssier

RWTH Aachen University, III. Physikalisches Institut B, Aachen, Germany

M. Bontenackels, V. Cherepanov, M. Davids, M. Duda, G. Flügge, H. Geenen, M. Giffels, W. Haj Ahmad, D. Heydhausen, F. Hoehle, B. Kargoll, T. Kress, Y. Kuessel, A. Linn, A. Nowack, L. Perchalla, O. Pooth, J. Rennefeld, P. Sauerland, A. Stahl, D. Tornier, M.H. Zoeller

Deutsches Elektronen-Synchrotron, Hamburg, Germany

M. Aldaya Martin, W. Behrenhoff, U. Behrens, M. Bergholz¹², A. Bethani, K. Borras, A. Cakir, A. Campbell, E. Castro, D. Dammann, G. Eckerlin, D. Eckstein, A. Flossdorf, G. Flucke, A. Geiser, J. Hauk, H. Jung¹, M. Kasemann, P. Katsas, C. Kleinwort, H. Kluge, A. Knutsson, M. Krämer, D. Krücker, E. Kuznetsova, W. Lange, W. Lohmann¹², R. Mankel, M. Marienfeld, I.-A. Melzer-Pellmann, A.B. Meyer, J. Mnich, A. Mussgiller, J. Olzem, A. Petrukhin, D. Pitzl, A. Raspereza, M. Rosin, R. Schmidt¹², T. Schoerner-Sadenius, N. Sen, A. Spiridonov, M. Stein, J. Tomaszewska, R. Walsh, C. Wissing

University of Hamburg, Hamburg, Germany

C. Autermann, V. Blobel, S. Bobrovskyi, J. Draeger, H. Enderle, U. Gebbert, M. Görner,

T. Hermanns, K. Kaschube, G. Kaussen, H. Kirschenmann, R. Klanner, J. Lange, B. Mura, S. Naumann-Emme, F. Nowak, N. Pietsch, C. Sander, H. Schettler, P. Schleper, E. Schlieckau, M. Schröder, T. Schum, H. Stadie, G. Steinbrück, J. Thomsen

Institut für Experimentelle Kernphysik, Karlsruhe, Germany

C. Barth, J. Bauer, J. Berger, V. Buege, T. Chwalek, W. De Boer, A. Dierlamm, G. Dirkes, M. Feindt, J. Gruschke, C. Hackstein, F. Hartmann, M. Heinrich, H. Held, K.H. Hoffmann, S. Honc, I. Katkov¹³, J.R. Komaragiri, T. Kuhr, D. Martschei, S. Mueller, Th. Müller, M. Niegel, O. Oberst, A. Oehler, J. Ott, T. Peiffer, G. Quast, K. Rabbertz, F. Ratnikov, N. Ratnikova, M. Renz, C. Saout, A. Scheurer, P. Schieferdecker, F.-P. Schilling, G. Schott, H.J. Simonis, F.M. Stober, D. Troendle, J. Wagner-Kuhr, T. Weiler, M. Zeise, V. Zhukov¹³, E.B. Ziebarth

Institute of Nuclear Physics "Demokritos", Aghia Paraskevi, Greece

G. Daskalakis, T. Geralis, S. Kesisoglou, A. Kyriakis, D. Loukas, I. Manolakos, A. Markou, C. Markou, C. Mavrommatis, E. Ntomari, E. Petrakou

University of Athens, Athens, Greece

L. Gouskos, T.J. Mertzimekis, A. Panagiotou, N. Saoulidou, E. Stiliaris

University of Ioánnina, Ioánnina, Greece

I. Evangelou, C. Foudas, P. Kokkas, N. Manthos, I. Papadopoulos, V. Patras, F.A. Triantis

KFKI Research Institute for Particle and Nuclear Physics, Budapest, Hungary

A. Aranyi, G. Bencze, L. Boldizsar, C. Hajdu¹, P. Hidas, D. Horvath¹⁴, A. Kapusi, K. Krajczar¹⁵, F. Sikler¹, G.I. Veres¹⁵, G. Vesztergombi¹⁵

Institute of Nuclear Research ATOMKI, Debrecen, Hungary

N. Beni, J. Molnar, J. Palinkas, Z. Szillasi, V. Veszpremi

University of Debrecen, Debrecen, Hungary

P. Raics, Z.L. Trocsanyi, B. Ujvari

Panjab University, Chandigarh, India

S.B. Beri, V. Bhatnagar, N. Dhingra, R. Gupta, M. Jindal, M. Kaur, J.M. Kohli, M.Z. Mehta, N. Nishu, L.K. Saini, A. Sharma, A.P. Singh, J. Singh, S.P. Singh

University of Delhi, Delhi, India

S. Ahuja, B.C. Choudhary, P. Gupta, A. Kumar, A. Kumar, S. Malhotra, M. Naimuddin, K. Ranjan, R.K. Shivpuri

Saha Institute of Nuclear Physics, Kolkata, India

S. Banerjee, S. Bhattacharya, S. Dutta, B. Gomber, S. Jain, S. Jain, R. Khurana, S. Sarkar

Bhabha Atomic Research Centre, Mumbai, India

R.K. Choudhury, D. Dutta, S. Kailas, V. Kumar, P. Mehta, A.K. Mohanty¹, L.M. Pant, P. Shukla

Tata Institute of Fundamental Research - EHEP, Mumbai, India

T. Aziz, M. Guchait¹⁶, A. Gurtu, M. Maity¹⁷, D. Majumder, G. Majumder, K. Mazumdar, G.B. Mohanty, A. Saha, K. Sudhakar, N. Wickramage

Tata Institute of Fundamental Research - HECR, Mumbai, India

S. Banerjee, S. Dugad, N.K. Mondal

Institute for Research and Fundamental Sciences (IPM), Tehran, Iran

H. Arfaei, H. Bakhshiansohi¹⁸, S.M. Etesami, A. Fahim¹⁸, M. Hashemi, H. Hesari, A. Jafari¹⁸,

M. Khakzad, A. Mohammadi¹⁹, M. Mohammadi Najafabadi, S. Paktinat Mehdiabadi, B. Safarzadeh, M. Zeinali²⁰

INFN Sezione di Bari ^a, Università di Bari ^b, Politecnico di Bari ^c, Bari, Italy

M. Abbrescia^{a,b}, L. Barbone^{a,b}, C. Calabria^{a,b}, A. Colaleo^a, D. Creanza^{a,c}, N. De Filippis^{a,c,1}, M. De Palma^{a,b}, L. Fiore^a, G. Iaselli^{a,c}, L. Lusito^{a,b}, G. Maggi^{a,c}, M. Maggi^a, N. Manna^{a,b}, B. Marangelli^{a,b}, S. My^{a,c}, S. Nuzzo^{a,b}, N. Pacifico^{a,b}, G.A. Pierro^a, A. Pompili^{a,b}, G. Pugliese^{a,c}, F. Romano^{a,c}, G. Roselli^{a,b}, G. Selvaggi^{a,b}, L. Silvestris^a, R. Trentadue^a, S. Tuppiti^{a,b}, G. Zito^a

INFN Sezione di Bologna ^a, Università di Bologna ^b, Bologna, Italy

G. Abbiendi^a, A.C. Benvenuti^a, D. Bonacorsi^a, S. Braibant-Giacomelli^{a,b}, L. Brigliadori^a, P. Capiluppi^{a,b}, A. Castro^{a,b}, F.R. Cavallo^a, M. Cuffiani^{a,b}, G.M. Dallavalle^a, F. Fabbri^a, A. Fanfani^{a,b}, D. Fasanella^a, P. Giacomelli^a, M. Giunta^a, C. Grandi^a, S. Marcellini^a, G. Masetti^b, M. Meneghelli^{a,b}, A. Montanari^a, F.L. Navarria^{a,b}, F. Odoricci^a, A. Perrotta^a, F. Primavera^a, A.M. Rossi^{a,b}, T. Rovelli^{a,b}, G. Siroli^{a,b}, R. Travaglini^{a,b}

INFN Sezione di Catania ^a, Università di Catania ^b, Catania, Italy

S. Albergo^{a,b}, G. Cappello^{a,b}, M. Chiorboli^{a,b,1}, S. Costa^{a,b}, R. Potenza^{a,b}, A. Tricomi^{a,b}, C. Tuve^{a,b}

INFN Sezione di Firenze ^a, Università di Firenze ^b, Firenze, Italy

G. Barbagli^a, V. Ciulli^{a,b}, C. Civinini^a, R. D'Alessandro^{a,b}, E. Focardi^{a,b}, S. Frosali^{a,b}, E. Gallo^a, S. Gonzi^{a,b}, P. Lenzi^{a,b}, M. Meschini^a, S. Paoletti^a, G. Sguazzoni^a, A. Tropiano^{a,1}

INFN Laboratori Nazionali di Frascati, Frascati, Italy

L. Benussi, S. Bianco, S. Colafranceschi²¹, F. Fabbri, D. Piccolo

INFN Sezione di Genova, Genova, Italy

P. Fabbriatore, R. Musenich

INFN Sezione di Milano-Bicocca ^a, Università di Milano-Bicocca ^b, Milano, Italy

A. Benaglia^{a,b}, F. De Guio^{a,b,1}, L. Di Matteo^{a,b}, S. Gennai¹, A. Ghezzi^{a,b}, S. Malvezzi^a, A. Martelli^{a,b}, A. Massironi^{a,b}, D. Menasce^a, L. Moroni^a, M. Paganoni^{a,b}, D. Pedrini^a, S. Ragazzi^{a,b}, N. Redaelli^a, S. Sala^a, T. Tabarelli de Fatis^{a,b}

INFN Sezione di Napoli ^a, Università di Napoli "Federico II" ^b, Napoli, Italy

S. Buontempo^a, C.A. Carrillo Montoya^{a,1}, N. Cavallo^{a,22}, A. De Cosa^{a,b}, F. Fabozzi^{a,22}, A.O.M. Iorio^{a,1}, L. Lista^a, M. Merola^{a,b}, P. Paolucci^a

INFN Sezione di Padova ^a, Università di Padova ^b, Università di Trento (Trento) ^c, Padova, Italy

P. Azzi^a, N. Bacchetta^a, P. Bellan^{a,b}, D. Bisello^{a,b}, A. Branca^a, R. Carlin^{a,b}, P. Checchia^a, T. Dorigo^a, U. Dosselli^a, F. Fanzago^a, F. Gasparini^{a,b}, U. Gasparini^{a,b}, A. Gozzelino, S. Lacaprara^{a,23}, I. Lazzizzera^{a,c}, M. Margoni^{a,b}, M. Mazzucato^a, A.T. Meneguzzo^{a,b}, M. Nespolo^{a,1}, L. Perrozzi^{a,1}, N. Pozzobon^{a,b}, P. Ronchese^{a,b}, F. Simonetto^{a,b}, E. Torassa^a, M. Tosi^{a,b}, S. Vanini^{a,b}, P. Zotto^{a,b}, G. Zumerle^{a,b}

INFN Sezione di Pavia ^a, Università di Pavia ^b, Pavia, Italy

P. Baesso^{a,b}, U. Berzano^a, S.P. Ratti^{a,b}, C. Riccardi^{a,b}, P. Torre^{a,b}, P. Vitulo^{a,b}, C. Viviani^{a,b}

INFN Sezione di Perugia ^a, Università di Perugia ^b, Perugia, Italy

M. Biasini^{a,b}, G.M. Bilei^a, B. Caponeri^{a,b}, L. Fano^{a,b}, P. Lariccia^{a,b}, A. Lucaroni^{a,b,1}, G. Mantovani^{a,b}, M. Menichelli^a, A. Nappi^{a,b}, F. Romeo^{a,b}, A. Santocchia^{a,b}, S. Taroni^{a,b,1}, M. Valdata^{a,b}

INFN Sezione di Pisa ^a, Università di Pisa ^b, Scuola Normale Superiore di Pisa ^c, Pisa, Italy
 P. Azzurri^{a,c}, G. Bagliesi^a, J. Bernardini^{a,b}, T. Boccali^a, G. Broccolo^{a,c}, R. Castaldi^a,
 R.T. D'Agnolo^{a,c}, R. Dell'Orso^a, F. Fiori^{a,b}, L. Foà^{a,c}, A. Giassi^a, A. Kraan^a, F. Ligabue^{a,c},
 T. Lomtadze^a, L. Martini^{a,24}, A. Messineo^{a,b}, F. Palla^a, F. Palmonari, G. Segneri^a, A.T. Serban^a,
 P. Spagnolo^a, R. Tenchini^a, G. Tonelli^{a,b,1}, A. Venturi^{a,1}, P.G. Verdini^a

INFN Sezione di Roma ^a, Università di Roma "La Sapienza" ^b, Roma, Italy
 L. Barone^{a,b}, F. Cavallari^a, D. Del Re^{a,b}, E. Di Marco^{a,b}, M. Diemoz^a, D. Franci^{a,b}, M. Grassi^{a,1},
 E. Longo^{a,b}, P. Meridiani, S. Nourbakhsh^a, G. Organtini^{a,b}, F. Pandolfi^{a,b,1}, R. Paramatti^a,
 S. Rahatlou^{a,b}, M. Sigamani^a

INFN Sezione di Torino ^a, Università di Torino ^b, Università del Piemonte Orientale (Novara) ^c, Torino, Italy

N. Amapane^{a,b}, R. Arcidiacono^{a,c}, S. Argiro^{a,b}, M. Arneodo^{a,c}, C. Biino^a, C. Botta^{a,b,1},
 N. Cartiglia^a, R. Castello^{a,b}, M. Costa^{a,b}, N. Demaria^a, A. Graziano^{a,b,1}, C. Mariotti^a, S. Maselli^a,
 E. Migliore^{a,b}, V. Monaco^{a,b}, M. Musich^a, M.M. Obertino^{a,c}, N. Pastrone^a, M. Pelliccioni^{a,b},
 A. Potenza^{a,b}, A. Romero^{a,b}, M. Ruspà^{a,c}, R. Sacchi^{a,b}, V. Sola^{a,b}, A. Solano^{a,b}, A. Staiano^a,
 A. Vilela Pereira^a

INFN Sezione di Trieste ^a, Università di Trieste ^b, Trieste, Italy

S. Belforte^a, F. Cossutti^a, G. Della Ricca^{a,b}, B. Gobbo^a, M. Marone^{a,b}, D. Montanino^{a,b}, A. Penzo^a

Kangwon National University, Chunchon, Korea

S.G. Heo, S.K. Nam

Kyungpook National University, Daegu, Korea

S. Chang, J. Chung, D.H. Kim, G.N. Kim, J.E. Kim, D.J. Kong, H. Park, S.R. Ro, D.C. Son, T. Son

Chonnam National University, Institute for Universe and Elementary Particles, Kwangju, Korea

J.Y. Kim, Zero J. Kim, S. Song

Konkuk University, Seoul, Korea

H.Y. Jo

Korea University, Seoul, Korea

S. Choi, D. Gyun, B. Hong, M. Jo, H. Kim, J.H. Kim, T.J. Kim, K.S. Lee, D.H. Moon, S.K. Park,
 E. Seo, K.S. Sim

University of Seoul, Seoul, Korea

M. Choi, S. Kang, H. Kim, C. Park, I.C. Park, S. Park, G. Ryu

Sungkyunkwan University, Suwon, Korea

Y. Cho, Y. Choi, Y.K. Choi, J. Goh, M.S. Kim, B. Lee, J. Lee, S. Lee, H. Seo, I. Yu

Vilnius University, Vilnius, Lithuania

M.J. Bilinskas, I. Grigelionis, M. Janulis, D. Martisiute, P. Petrov, M. Polujanskas, T. Sabonis

Centro de Investigacion y de Estudios Avanzados del IPN, Mexico City, Mexico

H. Castilla-Valdez, E. De La Cruz-Burelo, I. Heredia-de La Cruz, R. Lopez-Fernandez,
 R. Magaña Villalba, J. Martínez-Ortega, A. Sánchez-Hernández, L.M. Villasenor-Cendejas

Universidad Iberoamericana, Mexico City, Mexico

S. Carrillo Moreno, F. Vazquez Valencia

Benemerita Universidad Autonoma de Puebla, Puebla, Mexico

H.A. Salazar Ibarguen

Universidad Autónoma de San Luis Potosí, San Luis Potosí, Mexico

E. Casimiro Linares, A. Morelos Pineda, M.A. Reyes-Santos

University of Auckland, Auckland, New Zealand

D. Krofcheck, J. Tam

University of Canterbury, Christchurch, New Zealand

P.H. Butler, R. Doesburg, H. Silverwood

National Centre for Physics, Quaid-I-Azam University, Islamabad, Pakistan

M. Ahmad, I. Ahmed, M.H. Ansari, M.I. Asghar, H.R. Hoorani, S. Khalid, W.A. Khan, T. Khurshid, S. Qazi, M.A. Shah, M. Shoaib

Institute of Experimental Physics, Faculty of Physics, University of Warsaw, Warsaw, Poland

G. Brona, M. Cwiok, W. Dominik, K. Doroba, A. Kalinowski, M. Konecki, J. Krolikowski

Soltan Institute for Nuclear Studies, Warsaw, Poland

T. Frueboes, R. Gokieli, M. Górski, M. Kazana, K. Nawrocki, K. Romanowska-Rybinska, M. Szleper, G. Wrochna, P. Zalewski

Laboratório de Instrumentação e Física Experimental de Partículas, Lisboa, PortugalN. Almeida, P. Bargassa, A. David, P. Faccioli, P.G. Ferreira Parracho, M. Gallinaro¹, P. Musella, A. Nayak, J. Pela¹, P.Q. Ribeiro, J. Seixas, J. Varela**Joint Institute for Nuclear Research, Dubna, Russia**

S. Afanasiev, I. Belotelov, P. Bunin, M. Gavrilenko, I. Golutvin, A. Kamenev, V. Karjavin, G. Kozlov, A. Lanev, P. Moisenz, V. Palichik, V. Perelygin, S. Shmatov, V. Smirnov, A. Volodko, A. Zarubin

Petersburg Nuclear Physics Institute, Gatchina (St Petersburg), Russia

V. Golovtsov, Y. Ivanov, V. Kim, P. Levchenko, V. Murzin, V. Oreshkin, I. Smirnov, V. Sulimov, L. Uvarov, S. Vavilov, A. Vorobyev, An. Vorobyev

Institute for Nuclear Research, Moscow, Russia

Yu. Andreev, A. Dermenev, S. Gninenko, N. Golubev, M. Kirsanov, N. Krasnikov, V. Matveev, A. Pashenkov, A. Toropin, S. Troitsky

Institute for Theoretical and Experimental Physics, Moscow, RussiaV. Epshteyn, M. Erofeeva, V. Gavrilov, V. Kaftanov[†], M. Kossov¹, A. Krokhotin, N. Lychkovskaya, V. Popov, G. Safronov, S. Semenov, V. Stolin, E. Vlasov, A. Zhokin**Moscow State University, Moscow, Russia**A. Belyaev, E. Boos, M. Dubinin³, L. Dudko, A. Ershov, A. Gribushin, O. Kodolova, I. Lokhtin, A. Markina, S. Obraztsov, M. Perfilov, S. Petrushanko, L. Sarycheva, V. Savrin, A. Snigirev**P.N. Lebedev Physical Institute, Moscow, Russia**

V. Andreev, M. Azarkin, I. Dremin, M. Kirakosyan, A. Leonidov, G. Mesyats, S.V. Rusakov, A. Vinogradov

State Research Center of Russian Federation, Institute for High Energy Physics, Protvino, RussiaI. Azhgirey, I. Bayshev, S. Bitioukov, V. Grishin¹, V. Kachanov, D. Konstantinov, A. Korablev,

V. Krychkin, V. Petrov, R. Ryutin, A. Sobol, L. Tourtchanovitch, S. Troshin, N. Tyurin, A. Uzunian, A. Volkov

University of Belgrade, Faculty of Physics and Vinca Institute of Nuclear Sciences, Belgrade, Serbia

P. Adzic²⁵, M. Djordjevic, D. Krpic²⁵, J. Milosevic

Centro de Investigaciones Energéticas Medioambientales y Tecnológicas (CIEMAT), Madrid, Spain

M. Aguilar-Benitez, J. Alcaraz Maestre, P. Arce, C. Battilana, E. Calvo, M. Cerrada, M. Chamizo Llatas, N. Colino, B. De La Cruz, A. Delgado Peris, C. Diez Pardos, D. Domínguez Vázquez, C. Fernandez Bedoya, J.P. Fernández Ramos, A. Ferrando, J. Flix, M.C. Fouz, P. Garcia-Abia, O. Gonzalez Lopez, S. Goy Lopez, J.M. Hernandez, M.I. Josa, G. Merino, J. Puerta Pelayo, I. Redondo, L. Romero, J. Santaolalla, M.S. Soares, C. Willmott

Universidad Autónoma de Madrid, Madrid, Spain

C. Albajar, G. Codispoti, J.F. de Trocóniz

Universidad de Oviedo, Oviedo, Spain

J. Cuevas, J. Fernandez Menendez, S. Folgueras, I. Gonzalez Caballero, L. Lloret Iglesias, J.M. Vizan Garcia

Instituto de Física de Cantabria (IFCA), CSIC-Universidad de Cantabria, Santander, Spain

J.A. Brochero Cifuentes, I.J. Cabrillo, A. Calderon, S.H. Chuang, J. Duarte Campderros, M. Felcini²⁶, M. Fernandez, G. Gomez, J. Gonzalez Sanchez, C. Jorda, P. Lobelle Pardo, A. Lopez Virto, J. Marco, R. Marco, C. Martinez Rivero, F. Matorras, F.J. Munoz Sanchez, J. Piedra Gomez²⁷, T. Rodrigo, A.Y. Rodríguez-Marrero, A. Ruiz-Jimeno, L. Scodellaro, M. Sobron Sanudo, I. Vila, R. Vilar Cortabitarte

CERN, European Organization for Nuclear Research, Geneva, Switzerland

D. Abbaneo, E. Auffray, G. Auzinger, P. Baillon, A.H. Ball, D. Barney, A.J. Bell²⁸, D. Benedetti, C. Bernet⁴, W. Bialas, P. Bloch, A. Bocci, S. Bolognesi, M. Bona, H. Breuker, K. Bunkowski, T. Camporesi, G. Cerminara, T. Christiansen, J.A. Coarasa Perez, B. Curé, D. D'Enterria, A. De Roeck, S. Di Guida, N. Dupont-Sagorin, A. Elliott-Peisert, B. Frisch, W. Funk, A. Gaddi, G. Georgiou, H. Gerwig, D. Gigi, K. Gill, D. Giordano, F. Glege, R. Gomez-Reino Garrido, M. Gouzevitch, P. Govoni, S. Gowdy, R. Guida, L. Guiducci, M. Hansen, C. Hartl, J. Harvey, J. Hegeman, B. Hegner, H.F. Hoffmann, V. Innocente, P. Janot, K. Kaadze, E. Karavakis, P. Lecoq, C. Lourenço, T. Mäki, M. Malberti, L. Malgeri, M. Mannelli, L. Masetti, A. Maurisset, F. Meijers, S. Mersi, E. Meschi, R. Moser, M.U. Mozer, M. Mulders, E. Nesvold, M. Nguyen, T. Orimoto, L. Orsini, E. Palencia Cortezon, E. Perez, A. Petrilli, A. Pfeiffer, M. Pierini, M. Pimiä, D. Piparo, G. Polese, L. Quertenmont, A. Racz, W. Reece, J. Rodrigues Antunes, G. Rolandi²⁹, T. Rommerskirchen, C. Rovelli³⁰, M. Rovere, H. Sakulin, C. Schäfer, C. Schwick, I. Segoni, A. Sharma, P. Siegrist, P. Silva, M. Simon, P. Sphicas³¹, D. Spiga, M. Spiropulu³, M. Stoye, A. Tsiros, P. Vichoudis, H.K. Wöhri, S.D. Worm, W.D. Zeuner

Paul Scherrer Institut, Villigen, Switzerland

W. Bertl, K. Deiters, W. Erdmann, K. Gabathuler, R. Horisberger, Q. Ingram, H.C. Kaestli, S. König, D. Kotlinski, U. Langenegger, F. Meier, D. Renker, T. Rohe, J. Sibille³²

Institute for Particle Physics, ETH Zurich, Zurich, Switzerland

L. Bäni, P. Bortignon, L. Caminada³³, B. Casal, N. Chanon, Z. Chen, S. Cittolin, G. Dissertori, M. Dittmar, J. Eugster, K. Freudenreich, C. Grab, W. Hintz, P. Lecomte, W. Lustermann, C. Marchica³³, P. Martinez Ruiz del Arbol, P. Milenovic³⁴, F. Moortgat, C. Nägeli³³, P. Nef,

F. Nessi-Tedaldi, L. Pape, F. Pauss, T. Punz, A. Rizzi, F.J. Ronga, M. Rossini, L. Sala, A.K. Sanchez, M.-C. Sawley, A. Starodumov³⁵, B. Stieger, M. Takahashi, L. Tauscher[†], A. Thea, K. Theofilatos, D. Treille, C. Urscheler, R. Wallny, M. Weber, L. Wehrli, J. Weng

Universität Zürich, Zurich, Switzerland

E. Aguilo, C. Amsler, V. Chiochia, S. De Visscher, C. Favaro, M. Ivova Rikova, A. Jaeger, B. Millan Mejias, P. Otiougova, P. Robmann, A. Schmidt, H. Snoek

National Central University, Chung-Li, Taiwan

Y.H. Chang, K.H. Chen, C.M. Kuo, S.W. Li, W. Lin, Z.K. Liu, Y.J. Lu, D. Mekterovic, R. Volpe, S.S. Yu

National Taiwan University (NTU), Taipei, Taiwan

P. Bartalini, P. Chang, Y.H. Chang, Y.W. Chang, Y. Chao, K.F. Chen, W.-S. Hou, Y. Hsiung, K.Y. Kao, Y.J. Lei, R.-S. Lu, J.G. Shiu, Y.M. Tzeng, X. Wan, M. Wang

Cukurova University, Adana, Turkey

A. Adiguzel, M.N. Bakirci³⁶, S. Cerci³⁷, C. Dozen, I. Dumanoglu, E. Eskut, S. Girgis, G. Gokbulut, I. Hos, E.E. Kangal, A. Kayis Topaksu, G. Onengut, K. Ozdemir, S. Ozturk³⁸, A. Polatoz, K. Sogut³⁹, D. Sunar Cerci³⁷, B. Tali³⁷, H. Topakli³⁶, D. Uzun, L.N. Vergili, M. Vergili

Middle East Technical University, Physics Department, Ankara, Turkey

I.V. Akin, T. Aliev, B. Bilin, S. Bilmis, M. Deniz, H. Gamsizkan, A.M. Guler, K. Ocalan, A. Ozpineci, M. Serin, R. Sever, U.E. Surat, M. Yalvac, E. Yildirim, M. Zeyrek

Bogazici University, Istanbul, Turkey

M. Deliomeroglu, D. Demir⁴⁰, E. Gülmez, B. Isildak, M. Kaya⁴¹, O. Kaya⁴¹, M. Özbek, S. Ozkorucuklu⁴², N. Sonmez⁴³

National Scientific Center, Kharkov Institute of Physics and Technology, Kharkov, Ukraine

L. Levchuk

University of Bristol, Bristol, United Kingdom

F. Bostock, J.J. Brooke, T.L. Cheng, E. Clement, D. Cussans, R. Frazier, J. Goldstein, M. Grimes, D. Hartley, G.P. Heath, H.F. Heath, L. Kreczko, S. Metson, D.M. Newbold⁴⁴, K. Nirunpong, A. Poll, S. Senkin, V.J. Smith

Rutherford Appleton Laboratory, Didcot, United Kingdom

L. Basso⁴⁵, K.W. Bell, A. Belyaev⁴⁵, C. Brew, R.M. Brown, B. Camanzi, D.J.A. Cockerill, J.A. Coughlan, K. Harder, S. Harper, J. Jackson, B.W. Kennedy, E. Olaiya, D. Petyt, B.C. Radburn-Smith, C.H. Shepherd-Themistocleous, I.R. Tomalin, W.J. Womersley

Imperial College, London, United Kingdom

R. Bainbridge, G. Ball, J. Ballin, R. Beuselinck, O. Buchmuller, D. Colling, N. Cripps, M. Cutajar, G. Davies, M. Della Negra, W. Ferguson, J. Fulcher, D. Futyan, A. Gilbert, A. Guneratne Bryer, G. Hall, Z. Hatherell, J. Hays, G. Iles, M. Jarvis, G. Karapostoli, L. Lyons, B.C. MacEvoy, A.-M. Magnan, J. Marrouche, B. Mathias, R. Nandi, J. Nash, A. Nikitenko³⁵, A. Papageorgiou, M. Pesaresi, K. Petridis, M. Pioppi⁴⁶, D.M. Raymond, S. Rogerson, N. Rompotis, A. Rose, M.J. Ryan, C. Seez, P. Sharp, A. Sparrow, A. Tapper, S. Tourneur, M. Vazquez Acosta, T. Virdee, S. Wakefield, N. Wardle, D. Wardrope, T. Whyntie

Brunel University, Uxbridge, United Kingdom

M. Barrett, M. Chadwick, J.E. Cole, P.R. Hobson, A. Khan, P. Kyberd, D. Leslie, W. Martin, I.D. Reid, L. Teodorescu

Baylor University, Waco, USA

K. Hatakeyama, H. Liu

The University of Alabama, Tuscaloosa, USA

C. Henderson

Boston University, Boston, USA

T. Bose, E. Carrera Jarrin, C. Fantasia, A. Heister, J. St. John, P. Lawson, D. Lazic, J. Rohlf, D. Sperka, L. Sulak

Brown University, Providence, USA

A. Avetisyan, S. Bhattacharya, J.P. Chou, D. Cutts, A. Ferapontov, U. Heintz, S. Jabeen, G. Kukartsev, G. Landsberg, M. Luk, M. Narain, D. Nguyen, M. Segala, T. Sinthuprasith, T. Speer, K.V. Tsang

University of California, Davis, Davis, USA

R. Breedon, G. Breto, M. Calderon De La Barca Sanchez, S. Chauhan, M. Chertok, J. Conway, R. Conway, P.T. Cox, J. Dolen, R. Erbacher, E. Friis, W. Ko, A. Kopecky, R. Lander, H. Liu, S. Maruyama, T. Miceli, M. Nikolic, D. Pellett, J. Robles, B. Rutherford, S. Salur, T. Schwarz, M. Searle, J. Smith, M. Squires, M. Tripathi, R. Vasquez Sierra, C. Veelken

University of California, Los Angeles, Los Angeles, USA

V. Andreev, K. Arisaka, D. Cline, R. Cousins, A. Deisher, J. Duris, S. Erhan, C. Farrell, J. Hauser, M. Ignatenko, C. Jarvis, C. Plager, G. Rakness, P. Schlein[†], J. Tucker, V. Valuev

University of California, Riverside, Riverside, USA

J. Babb, A. Chandra, R. Clare, J. Ellison, J.W. Gary, F. Giordano, G. Hanson, G.Y. Jeng, S.C. Kao, F. Liu, H. Liu, O.R. Long, A. Luthra, H. Nguyen, S. Paramesvaran, B.C. Shen[†], R. Stringer, J. Sturdy, S. Sumowidagdo, R. Wilken, S. Wimpenny

University of California, San Diego, La Jolla, USA

W. Andrews, J.G. Branson, G.B. Cerati, D. Evans, F. Golf, A. Holzner, R. Kelley, M. Lebourgeois, J. Letts, B. Mangano, S. Padhi, C. Palmer, G. Petrucciani, H. Pi, M. Pieri, R. Ranieri, M. Sani, V. Sharma, S. Simon, E. Sudano, M. Tadel, Y. Tu, A. Vartak, S. Wasserbaech⁴⁷, F. Würthwein, A. Yagil, J. Yoo

University of California, Santa Barbara, Santa Barbara, USA

D. Barge, R. Bellan, C. Campagnari, M. D'Alfonso, T. Danielson, K. Flowers, P. Geffert, J. Incandela, C. Justus, P. Kalavase, S.A. Koay, D. Kovalskyi¹, V. Krutelyov, S. Lowette, N. Mccoll, E. Mullin, V. Pavlunin, F. Rebassoo, J. Ribnik, J. Richman, R. Rossin, D. Stuart, W. To, J.R. Vlimant, C. West

California Institute of Technology, Pasadena, USA

A. Apresyan, A. Bornheim, J. Bunn, Y. Chen, M. Gataullin, Y. Ma, A. Mott, H.B. Newman, C. Rogan, K. Shin, V. Timciuc, P. Traczyk, J. Veverka, R. Wilkinson, Y. Yang, R.Y. Zhu

Carnegie Mellon University, Pittsburgh, USA

B. Akgun, R. Carroll, T. Ferguson, Y. Iiyama, D.W. Jang, S.Y. Jun, Y.F. Liu, M. Paulini, J. Russ, H. Vogel, I. Vorobiev

University of Colorado at Boulder, Boulder, USA

J.P. Cumalat, M.E. Dinardo, B.R. Drell, C.J. Edelmaier, W.T. Ford, A. Gaz, B. Heyburn, E. Luiggi Lopez, U. Nauenberg, J.G. Smith, K. Stenson, K.A. Ulmer, S.R. Wagner, S.L. Zang

Cornell University, Ithaca, USA

L. Agostino, J. Alexander, A. Chatterjee, N. Eggert, L.K. Gibbons, B. Heltsley, K. Henriksson, W. Hopkins, A. Khukhunaishvili, B. Kreis, Y. Liu, G. Nicolas Kaufman, J.R. Patterson, D. Puigh, A. Ryd, M. Saelim, E. Salvati, X. Shi, W. Sun, W.D. Teo, J. Thom, J. Thompson, J. Vaughan, Y. Weng, L. Winstrom, P. Wittich

Fairfield University, Fairfield, USA

A. Biselli, G. Cirino, D. Winn

Fermi National Accelerator Laboratory, Batavia, USA

S. Abdullin, M. Albrow, J. Anderson, G. Apollinari, M. Atac, J.A. Bakken, L.A.T. Bauerdick, A. Beretvas, J. Berryhill, P.C. Bhat, I. Bloch, K. Burkett, J.N. Butler, V. Chetluru, H.W.K. Cheung, F. Chlebana, S. Cihangir, W. Cooper, D.P. Eartly, V.D. Elvira, S. Esen, I. Fisk, J. Freeman, Y. Gao, E. Gottschalk, D. Green, K. Gunthoti, O. Gutsche, J. Hanlon, R.M. Harris, J. Hirschauer, B. Hooberman, H. Jensen, M. Johnson, U. Joshi, R. Khatiwada, B. Klima, K. Kousouris, S. Kunori, S. Kwan, C. Leonidopoulos, P. Limon, D. Lincoln, R. Lipton, J. Lykken, K. Maeshima, J.M. Marraffino, D. Mason, P. McBride, T. Miao, K. Mishra, S. Mrenna, Y. Musienko⁴⁸, C. Newman-Holmes, V. O'Dell, J. Pivarski, R. Pordes, O. Prokofyev, E. Sexton-Kennedy, S. Sharma, W.J. Spalding, L. Spiegel, P. Tan, L. Taylor, S. Tkaczyk, L. Uplegger, E.W. Vaandering, R. Vidal, J. Whitmore, W. Wu, F. Yang, F. Yumiceva, J.C. Yun

University of Florida, Gainesville, USA

D. Acosta, P. Avery, D. Bourilkov, M. Chen, S. Das, M. De Gruttola, G.P. Di Giovanni, D. Dobur, A. Drozdetskiy, R.D. Field, M. Fisher, Y. Fu, I.K. Furic, J. Gartner, S. Goldberg, J. Hugon, B. Kim, J. Konigsberg, A. Korytov, A. Kropivnitskaya, T. Kypreos, J.F. Low, K. Matchev, G. Mitselmakher, L. Muniz, P. Myeonghun, C. Prescott, R. Remington, A. Rinkevicius, M. Schmitt, B. Scurlock, P. Sellers, N. Skhirtladze, M. Snowball, D. Wang, J. Yelton, M. Zakaria

Florida International University, Miami, USA

V. Gaultney, L.M. Lebolo, S. Linn, P. Markowitz, G. Martinez, J.L. Rodriguez

Florida State University, Tallahassee, USA

T. Adams, A. Askew, J. Bochenek, J. Chen, B. Diamond, S.V. Gleyzer, J. Haas, S. Hagopian, V. Hagopian, M. Jenkins, K.F. Johnson, H. Prosper, S. Sekmen, V. Veeraraghavan

Florida Institute of Technology, Melbourne, USA

M.M. Baarmand, B. Dorney, M. Hohlmann, H. Kalakhety, I. Vodopiyarov

University of Illinois at Chicago (UIC), Chicago, USA

M.R. Adams, I.M. Anghel, L. Apanasevich, Y. Bai, V.E. Bazterra, R.R. Betts, J. Callner, R. Cavanaugh, C. Dragoiu, L. Gauthier, C.E. Gerber, D.J. Hofman, S. Khalatyan, G.J. Kunde⁴⁹, F. Lacroix, M. Malek, C. O'Brien, C. Silkworth, C. Silvestre, A. Smoron, D. Strom, N. Varelas

The University of Iowa, Iowa City, USA

U. Akgun, E.A. Albayrak, B. Bilki, W. Clarida, F. Duru, C.K. Lae, E. McCliment, J.-P. Merlo, H. Mermerkaya⁵⁰, A. Mestvirishvili, A. Moeller, J. Nachtman, C.R. Newsom, E. Norbeck, J. Olson, Y. Onel, F. Ozok, S. Sen, J. Wetzel, T. Yetkin, K. Yi

Johns Hopkins University, Baltimore, USA

B.A. Barnett, B. Blumenfeld, A. Bonato, C. Eskew, D. Fehling, G. Giurgiu, A.V. Gritsan, Z.J. Guo, G. Hu, P. Maksimovic, S. Rappoccio, M. Swartz, N.V. Tran, A. Whitbeck

The University of Kansas, Lawrence, USA

P. Baringer, A. Bean, G. Benelli, O. Grachov, R.P. Kenny Iii, M. Murray, D. Noonan, S. Sanders, J.S. Wood, V. Zhukova

Kansas State University, Manhattan, USA

A.f. Barfuss, T. Bolton, I. Chakaberia, A. Ivanov, S. Khalil, M. Makouski, Y. Maravin, S. Shrestha, I. Svintradze, Z. Wan

Lawrence Livermore National Laboratory, Livermore, USA

J. Gronberg, D. Lange, D. Wright

University of Maryland, College Park, USA

A. Baden, M. Boutemour, S.C. Eno, D. Ferencek, J.A. Gomez, N.J. Hadley, R.G. Kellogg, M. Kirn, Y. Lu, A.C. Mignerey, K. Rossato, P. Rumerio, F. Santanastasio, A. Skuja, J. Temple, M.B. Tonjes, S.C. Tonwar, E. Twedt

Massachusetts Institute of Technology, Cambridge, USA

B. Alver, G. Bauer, J. Bendavid, W. Busza, E. Butz, I.A. Cali, M. Chan, V. Dutta, P. Everaerts, G. Gomez Ceballos, M. Goncharov, K.A. Hahn, P. Harris, Y. Kim, M. Klute, Y.-J. Lee, W. Li, C. Loizides, P.D. Luckey, T. Ma, S. Nahn, C. Paus, D. Ralph, C. Roland, G. Roland, M. Rudolph, G.S.F. Stephans, F. Stöckli, K. Sumorok, K. Sung, D. Velicanu, E.A. Wenger, R. Wolf, S. Xie, M. Yang, Y. Yilmaz, A.S. Yoon, M. Zanetti

University of Minnesota, Minneapolis, USA

S.I. Cooper, P. Cushman, B. Dahmes, A. De Benedetti, G. Franzoni, A. Gude, J. Haupt, K. Klapoetke, Y. Kubota, J. Mans, N. Pastika, V. Rekovic, R. Rusack, M. Sasseville, A. Singovsky, N. Tambe, J. Turkewitz

University of Mississippi, University, USA

L.M. Cremaldi, R. Godang, R. Kroeger, L. Perera, R. Rahmat, D.A. Sanders, D. Summers

University of Nebraska-Lincoln, Lincoln, USA

K. Bloom, S. Bose, J. Butt, D.R. Claes, A. Dominguez, M. Eads, P. Jindal, J. Keller, T. Kelly, I. Kravchenko, J. Lazo-Flores, H. Malbouisson, S. Malik, G.R. Snow

State University of New York at Buffalo, Buffalo, USA

U. Baur, A. Godshalk, I. Iashvili, S. Jain, A. Kharchilava, A. Kumar, S.P. Shipkowski, K. Smith

Northeastern University, Boston, USA

G. Alverson, E. Barberis, D. Baumgartel, O. Boeriu, M. Chasco, S. Reucroft, J. Swain, D. Trocino, D. Wood, J. Zhang

Northwestern University, Evanston, USA

A. Anastassov, A. Kubik, N. Mucia, N. Odell, R.A. Ofierzynski, B. Pollack, A. Pozdnyakov, M. Schmitt, S. Stoynev, M. Velasco, S. Won

University of Notre Dame, Notre Dame, USA

L. Antonelli, D. Berry, A. Brinkerhoff, M. Hildreth, C. Jessop, D.J. Karmgard, J. Kolb, T. Kolberg, K. Lannon, W. Luo, S. Lynch, N. Marinelli, D.M. Morse, T. Pearson, R. Ruchti, J. Slaunwhite, N. Valls, M. Wayne, J. Ziegler

The Ohio State University, Columbus, USA

B. Bylsma, L.S. Durkin, J. Gu, C. Hill, P. Killewald, K. Kotov, T.Y. Ling, M. Rodenburg, C. Vuosalo, G. Williams

Princeton University, Princeton, USA

N. Adam, E. Berry, P. Elmer, D. Gerbaudo, V. Halyo, P. Hebda, A. Hunt, E. Laird, D. Lopes

Pegna, D. Marlow, T. Medvedeva, M. Mooney, J. Olsen, P. Piroué, X. Quan, B. Safdi, H. Saka, D. Stickland, C. Tully, J.S. Werner, A. Zuranski

University of Puerto Rico, Mayaguez, USA

J.G. Acosta, X.T. Huang, A. Lopez, H. Mendez, S. Oliveros, J.E. Ramirez Vargas, A. Zatserklyaniy

Purdue University, West Lafayette, USA

E. Alagoz, V.E. Barnes, G. Bolla, L. Borrello, D. Bortoletto, M. De Mattia, A. Everett, A.F. Garfinkel, L. Gutay, Z. Hu, M. Jones, O. Koybasi, M. Kress, A.T. Laasanen, N. Leonardo, C. Liu, V. Maroussov, P. Merkel, D.H. Miller, N. Neumeister, I. Shipsey, D. Silvers, A. Svyatkovskiy, H.D. Yoo, J. Zablocki, Y. Zheng

Purdue University Calumet, Hammond, USA

S. Guragain, N. Parashar

Rice University, Houston, USA

A. Adair, C. Boulahouache, K.M. Ecklund, F.J.M. Geurts, B.P. Padley, R. Redjimi, J. Roberts, J. Zabel

University of Rochester, Rochester, USA

B. Betchart, A. Bodek, Y.S. Chung, R. Covarelli, P. de Barbaro, R. Demina, Y. Eshaq, H. Flacher, A. Garcia-Bellido, P. Goldenzweig, Y. Gotra, J. Han, A. Harel, D.C. Miner, D. Orbaker, G. Petrillo, W. Sakumoto, D. Vishnevskiy, M. Zielinski

The Rockefeller University, New York, USA

A. Bhatti, R. Ciesielski, L. Demortier, K. Goulios, G. Lungu, S. Malik, C. Mesropian

Rutgers, the State University of New Jersey, Piscataway, USA

S. Arora, O. Atramentov, A. Barker, C. Contreras-Campana, E. Contreras-Campana, D. Duggan, Y. Gershtein, R. Gray, E. Halkiadakis, D. Hidas, D. Hits, A. Lath, S. Panwalkar, R. Patel, A. Richards, K. Rose, S. Schnetzer, S. Somalwar, R. Stone, S. Thomas

University of Tennessee, Knoxville, USA

G. Cerizza, M. Hollingsworth, S. Spanier, Z.C. Yang, A. York

Texas A&M University, College Station, USA

R. Eusebi, W. Flanagan, J. Gilmore, A. Gurrola, T. Kamon, V. Khotilovich, R. Montalvo, I. Osipenkov, Y. Pakhotin, A. Safonov, S. Sengupta, I. Suarez, A. Tatarinov, D. Toback

Texas Tech University, Lubbock, USA

N. Akchurin, C. Bardak, J. Damgov, P.R. Duderu, C. Jeong, K. Kovitangoon, S.W. Lee, T. Libeiro, P. Mane, Y. Roh, A. Sill, I. Volobouev, R. Wigmans, E. Yazgan

Vanderbilt University, Nashville, USA

E. Appelt, E. Brownson, D. Engh, C. Florez, W. Gabella, M. Issah, W. Johns, C. Johnston, P. Kurt, C. Maguire, A. Melo, P. Sheldon, B. Snook, S. Tuo, J. Velkovska

University of Virginia, Charlottesville, USA

M.W. Arenton, M. Balazs, S. Boutle, B. Cox, B. Francis, S. Goadhouse, J. Goodell, R. Hirosky, A. Ledovskoy, C. Lin, C. Neu, J. Wood, R. Yohay

Wayne State University, Detroit, USA

S. Gollapinni, R. Harr, P.E. Karchin, C. Kottachchi Kankanamge Don, P. Lamichhane, M. Mattson, C. Milstène, A. Sakharov

University of Wisconsin, Madison, USA

M. Anderson, M. Bachtis, D. Belknap, J.N. Bellinger, D. Carlsmith, M. Cepeda, S. Dasu, J. Efron, L. Gray, K.S. Grogg, M. Grothe, R. Hall-Wilton, M. Herndon, A. Hervé, P. Klabbers, J. Klukas, A. Lanaro, C. Lazaridis, J. Leonard, R. Loveless, A. Mohapatra, I. Ojalvo, W. Parker, I. Ross, A. Savin, W.H. Smith, J. Swanson, M. Weinberg

†: Deceased

- 1: Also at CERN, European Organization for Nuclear Research, Geneva, Switzerland
- 2: Also at Universidade Federal do ABC, Santo Andre, Brazil
- 3: Also at California Institute of Technology, Pasadena, USA
- 4: Also at Laboratoire Leprince-Ringuet, Ecole Polytechnique, IN2P3-CNRS, Palaiseau, France
- 5: Also at Suez Canal University, Suez, Egypt
- 6: Also at British University, Cairo, Egypt
- 7: Also at Fayoum University, El-Fayoum, Egypt
- 8: Also at Ain Shams University, Cairo, Egypt
- 9: Also at Soltan Institute for Nuclear Studies, Warsaw, Poland
- 10: Also at Massachusetts Institute of Technology, Cambridge, USA
- 11: Also at Université de Haute-Alsace, Mulhouse, France
- 12: Also at Brandenburg University of Technology, Cottbus, Germany
- 13: Also at Moscow State University, Moscow, Russia
- 14: Also at Institute of Nuclear Research ATOMKI, Debrecen, Hungary
- 15: Also at Eötvös Loránd University, Budapest, Hungary
- 16: Also at Tata Institute of Fundamental Research - HECR, Mumbai, India
- 17: Also at University of Visva-Bharati, Santiniketan, India
- 18: Also at Sharif University of Technology, Tehran, Iran
- 19: Also at Shiraz University, Shiraz, Iran
- 20: Also at Isfahan University of Technology, Isfahan, Iran
- 21: Also at Facoltà Ingegneria Università di Roma, Roma, Italy
- 22: Also at Università della Basilicata, Potenza, Italy
- 23: Also at Laboratori Nazionali di Legnaro dell' INFN, Legnaro, Italy
- 24: Also at Università degli studi di Siena, Siena, Italy
- 25: Also at Faculty of Physics of University of Belgrade, Belgrade, Serbia
- 26: Also at University of California, Los Angeles, Los Angeles, USA
- 27: Also at University of Florida, Gainesville, USA
- 28: Also at Université de Genève, Geneva, Switzerland
- 29: Also at Scuola Normale e Sezione dell' INFN, Pisa, Italy
- 30: Also at INFN Sezione di Roma; Università di Roma "La Sapienza", Roma, Italy
- 31: Also at University of Athens, Athens, Greece
- 32: Also at The University of Kansas, Lawrence, USA
- 33: Also at Paul Scherrer Institut, Villigen, Switzerland
- 34: Also at University of Belgrade, Faculty of Physics and Vinca Institute of Nuclear Sciences, Belgrade, Serbia
- 35: Also at Institute for Theoretical and Experimental Physics, Moscow, Russia
- 36: Also at Gaziosmanpasa University, Tokat, Turkey
- 37: Also at Adiyaman University, Adiyaman, Turkey
- 38: Also at The University of Iowa, Iowa City, USA
- 39: Also at Mersin University, Mersin, Turkey
- 40: Also at Izmir Institute of Technology, Izmir, Turkey
- 41: Also at Kafkas University, Kars, Turkey
- 42: Also at Suleyman Demirel University, Isparta, Turkey

43: Also at Ege University, Izmir, Turkey

44: Also at Rutherford Appleton Laboratory, Didcot, United Kingdom

45: Also at School of Physics and Astronomy, University of Southampton, Southampton, United Kingdom

46: Also at INFN Sezione di Perugia; Università di Perugia, Perugia, Italy

47: Also at Utah Valley University, Orem, USA

48: Also at Institute for Nuclear Research, Moscow, Russia

49: Also at Los Alamos National Laboratory, Los Alamos, USA

50: Also at Erzincan University, Erzincan, Turkey